

# Design and Stability of Laminated Glass Beams and Cantilevers with Continuous Lateral Silicone Restraint

Richard Green <sup>a</sup>, Chiara Bedon <sup>b</sup>, Laura Galoupi <sup>c</sup>, Andrew Crosby <sup>d</sup>

a Green Facades PLLC, USA, [Richard@GreenFacadesLLC.com](mailto:Richard@GreenFacadesLLC.com)

b University of Trieste, Italy

c University of Parma, Italy

d RJC Engineers, Canada

## Abstract

The stability of monolithic glass beams is reasonably well defined; as an elastic material it behaves in a similar manner to other elastic materials such as steel, for which there are many equations of different forms which give similar results. Special care is required for continuous restraint to the tension flange. Equations presented in Australian Standard AS1288 Glass in Buildings – Selection and Installation have been used successfully for many years for monolithic fins when used with the strength model of AS1288 but require a more comprehensive approach when using laminated fins and/or strength models that allow higher levels of stress. A review of equations for cantilevers results in a wider range of approaches with significant variance between the outcomes of various published steel and glass standards. AS1288 has been used as the default standard for stability of glass fins, however for cantilevers it appears to have a misprint which has existed for decades. This paper presents strategies for determining the moment capacity of beams and cantilevers made of laminated glass with continuous flexible buckling restraints, such as structural silicone, which have initial imperfections and a known design strength capacity. Where multiple wave lengths form, the warping stiffness may contribute and formulations for rectangles are presented. The accuracy and validity of the approach is also assessed by means of comparisons with the outcomes of Finite Element numerical analyses.

## Keywords

Glass Structures, Glass Beams, Glass Cantilevers, Laminated Glass, Continuous Elastic Restraint, Imperfect Slender Beams

## Article Information

- Digital Object Identifier (DOI): [10.47982/cgc.9.599](https://doi.org/10.47982/cgc.9.599)
- Published by [Challenging Glass](#), on behalf of the author(s), at [Stichting OpenAccess](#).
- Published as part of the peer-reviewed [Challenging Glass Conference Proceedings](#), Volume 9, June 2024, [10.47982/cgc.9](https://doi.org/10.47982/cgc.9)
- Editors: Christian Louter, Freek Bos & Jan Belis
- This work is licensed under a [Creative Commons Attribution 4.0 International](#) (CC BY 4.0) license.
- Copyright © 2024 with the author(s)

## 1. Introduction

The use of laminated glass fins constitutes a recently emerging trend in the façade industry. In modern buildings, glass fins are used to support glazed façades and enhance their rigidity, and as supports for glazed roofs. As glass is brittle and can be damaged by non-design load events (e.g. impact), lamination is used to ensure a fail-safe response when one ply breaks. Due to their high slenderness, the design of glass fins requires particular attention to instability phenomena.

Currently, the main complete standard in this regard is the Australian Standard AS1288 (Appendix C), containing stability options for unrestrained monolithic beams (fins), beams with intermediate restraints, cantilevers, and continuously restrained beams. The continuously restrained beam case is perhaps the most common. The source of the formula for the continuously restrained case is not recorded in AS1288 and reputedly has origins in rectangular timber joist equations, which assume a rigid fixity to the diaphragm providing the restraint. However, when the restraint is flexible, such as in the common case where structural silicone is used, the formula can be non-conservative due to reduction of the elastic critical buckling load and development of secondary stresses from minor axis bending. The magnitude of the second-order stress is a function of the level of imperfection present in the construction. The AS1288 model generally provides adequate outcomes when used in combination with the design strength levels in AS1288, because the design stress limit for fins is relatively conservative, employing a glass type factor of 2.5 for fully tempered glass, instead of the value 4.0 in ASTM E1300, where glass type factor is the ratio of design capacity relative to that of annealed glass. If using higher stresses for design, without the 'buffer' of lower design stresses in AS1288, a more accurate formula for the stability is required and second-order effects need to be taken into consideration.

For cantilever beams, the equations for the Euler elastic critical moment was examined from multiple standards and sources, including AS 1288 Glass in Buildings, AISC 360 Specification for Structural Steel Buildings, NCCI SN006a-EN-EU Elastic Critical Moments of Cantilevers (reflecting Eurocode 3), AS 4100 *Steel Structures*, Timoshenko and Gere *Theory of Elastic Stability* (1956), Nethercott and Trahair (1976) and NASA N.A.C.A. *Technical Note No 601* (Dumont, 1937). From these various sources the relationship between the 'g factors' as presented in AS1288 and formulas presented elsewhere is clarified, which allows broader comparison, and a summary of the most useful sources is presented and discussed.

Kala (Kala, 2013) provides a derivation of moment capacity of beams for a given stress level and level of imperfection, geometric parameters, and elastic buckling moment. The derivation only holds true for the elastic range, but glass is elastic to fracture and, as rectangular fins are doubly symmetric, the compression limits and tension limits are the same magnitude (axial loads are not considered at this point). Finite element modelling has found the equation to have good agreement for the tension-controlled stress failure.

Bedon et al. (2015) demonstrate that a wavelength approach can be taken to glass fins with continuous elastic lateral restraints. The approach assumes the critical half-wavelength must be the length of member divided by an integer and requires testing for a number of integers to find the most critical (minimum) one. Bedon (2021) proposes separate equations for tension flange and compression flange with flexible continuous restraint. However, by selecting a suitable sign convention, the two equations can be merged in a unique approach, and further elaborated to capture the actual bending capacity, compared to rigid mechanical restraints (Bedon, 2021).

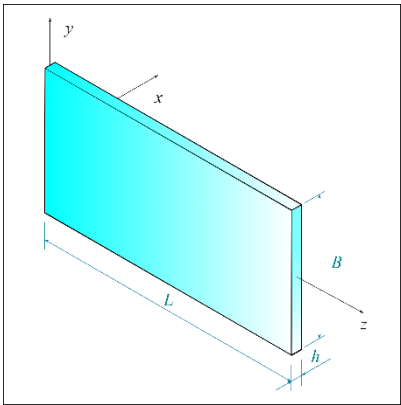
Laminated glass, composed of two or more glass plies bonded by polymeric interlayer(s), further adds to the complexity of the problem. The flexural and torsional response of this kind of composite is usually modelled by means of “effective thickness” methods, consisting in the definition of a monolithic “equivalent” element, of appropriate thickness, having the same flexural/torsional properties of the considered laminate. The effective thickness value depends on the mechanical and geometrical properties of both glass plies and interlayer(s), as well as by loading and boundary conditions. The Wölfel-Bennison effective thickness model in ASTM E1300 only correctly predicts the stiffness of simply supported beams under uniformly distributed load, with important inputs including: the length of the member, thickness of the interlayer and shear stiffness of the interlayer for a given temperature and duration. However, this model, developed for laminated glass elements under bending, significantly over-predicts the torsional stiffness of the glass fin and is non-conservative for stability calculations. Galuppi et al. (Galuppi, et al. 2013, 2014 and/or 2020) have developed an Enhanced Effective Thickness approach which includes additional parameters for torsional effective thickness that are strongly influenced by the width of the fin.

The proposed method predicts a more realistic capacity of glass beams and fins utilizing a combination of effective section properties (including torsional stiffnesses), a stability model (that accounts for flexibility of the restraint), and a method that considers second-order stresses (due to imperfections) in combination with the available design strength. Analytical predictions are validated towards Finite Element (FE) numerical analyses carried out in ABAQUS (Simulia, 2022) for a selection of geometrical and mechanical configurations.

## 2. Glossary and Conventions

| Description | Conventional US<br>Symbol<br>As used in paper<br>(Alt symbols not used in<br>brackets) | Conventional EU<br>Symbol<br>(and some prior<br>papers) | Conventional AU<br>Symbol<br>(AS 1288) |
|-------------|--|---|--|
| Axis system |  |   |  |
| Width       | $x$  | $y$   | $x$                                    |
| Height      | $y$  | $z$   | $y$                                    |
| Length      | $z$  | $x$   | $z$                                    |



|                           |     |          |     |
|---------------------------|-----|----------|-----|
| Breadth of beam           | $B$ |          | $b$ |
| Length of beam            | $L$ | $L, L_0$ | $L$ |
| Thickness: overall, plies | $h$ | $h$      | $t$ |



|                                    |          |        |            |
|------------------------------------|----------|--------|------------|
| Loading and boundary coefficient   |          |        |            |
| Bending                            | $\psi_b$ | $\psi$ |            |
| Torsion                            | $\psi_t$ |        |            |
| Material capacity reduction factor |          | $\Phi$ | $1/\gamma$ |
|                                    |          |        | $\Phi$     |

### 3. Method for Analysis of Glass Beams and Cantilevers

The method considers multiple components:

- The (Euler) elastic critical moment as a function of support conditions and load profile.
- The effective thickness of a member, taking into consideration the support conditions, load profile and buckling profile.
- The effects of continuous elastic restraint on the buckling profile and elastic critical buckling moment.
- The effects of imperfections which are amplified by applied loads.

### 4. Elastic Critical Buckling of Unrestrained Members

#### 4.1. Elastic Buckling Formulas for Unrestrained Beams

There are many available forms of the critical elastic buckling formula (also known as Euler Buckling Moment). The form used by the European steel code (EN 1993-1-1) was selected as a basis because it takes into consideration the position of load application and the moment profile and has a broad range of supporting documents. While US engineers may be more familiar with the AISC (ANSI/AISC 360) format with a  $C_b$  coefficient, accounting for the moment profile, the lack of a provision for load position was considered a disadvantage for slender rectangular fins without flanges and without torsional restraint at the lateral restraint, so it was not selected. The equation is re-written using the adopted axis convention.

$$M_{cr} = C_1 \frac{\pi^2 E I_y}{(kL)^2} \left\{ \sqrt{\left(\frac{k}{k_w}\right)^2 \frac{I_w}{J} + \frac{(kL)^2}{\pi^2 E I_y} + (C_2 y_a)^2} - C_2 y_a \right\} \quad (1)$$

where:

$C_1$  is a coefficient due to the moment profile (Table 1) (Note:  $C_1$  is similar to  $C_b$  coefficient (+/- 16% for cases in Table 1) as defined by the AISC standard (ANSI/AISC 360);

$C_2$  is a coefficient due to the moment profile (Table 1);

$E_g$  is the Young's Modulus of glass;

$G_g$  is the Shear Modulus of glass;

$I_y$  is the second moment of area about the minor axis;

$L$  is the distance between points of bracing of lateral torsional buckling;

$J$  is the Saint Venant's Torsional Stiffness, evaluated as

$J = (B \cdot h^3 / 3) (1 - 0.63 h/B)$  (The latter term allowing for beams that are not thin (AS 1288, 2021),

where

$B$  is the width of the beam,

$h$  is the thickness of the beam,

$y_a$  is the position of the load above the shear center when the load is acting toward the shear center, i.e.  $y_a$  is positive when the load is applied on the compression side of the beam.

$k$  and  $k_w$  are effective length factors. (The factor  $k$  refers to end rotation on plan. It is analogous to the ratio of the buckling length to the system length for a compression member.  $k$  should be taken as not less than 1 unless less than 1 can be justified. The factor  $k_w$  refers to end warping. Unless special provision for warping fixity is made,  $k_w$  should be taken as 1. (NCCI SN-003-EN-EU)

Table 1: Reference values for C1 and C2.

| Bending Moment   | C <sub>1</sub> | C <sub>2</sub> |
|--|----------------|----------------|
| Uniform (Constant)                                     | 1              | 0              |
| Linear (zero at midspan)                               | 2.7            | 0              |
| Parabolic (simply supported, zero at both extremities) | 1.127          | 0.454          |
| Parabolic (fixed end)                                  | 2.578          | 1.554          |
| Triangular (central point load, simply supported)      | 1.348          | 0.630          |
| Triangular (central point load, fixed end)             | 1,683          | 1.645          |

For additional coefficients, including beam segments or half-wave moment profile, reference can be made to NCCI SN-003-EN-EU.

#### 4.1.1. Elastic Critical Buckling Moment for Monolithic Beams

As glass beams are typically un-flanged and the buckling length is “long”, then the warping term is small and generally ignored, reducing the equation to the form shown in equation (2). (For continuously restrained beams with short half-wave lengths the warping stiffness can become appreciable, and the warping component is further discussed in that section.)

For monolithic glass beams, the critical buckling moment may be evaluated as

$$M_{CR} = C_1 \cdot \frac{(\pi^2 E_g I_y)}{L^2} \cdot \left[ \sqrt{(C_2 y_a)^2 + \frac{(G_g J L^2)}{\pi^2 E_g I_y}} - C_2 y_a \right] \quad (2)$$

#### 4.1.2. Elastic Critical Buckling Moment for Laminated Beams

For laminated glass beams, equation (2) takes the form:

$$M_{cr} = C_1 \frac{\pi^2 E_g I_{y_{eff}}}{L^2} \left[ \sqrt{(C_2 y_a)^2 + \frac{G_g J_{eff} L^2}{\pi^2 E_g I_{y_{eff}}}} - C_2 y_a \right] \quad (3)$$

where the subscript “eff” refers to the effective stiffness.

The Enhanced Effective Thickness (EET) method proposed by Galuppi et al. can be utilized to calculate the laminated stiffness for both lateral stiffness (Galuppi et al., 2014 and Galuppi et al. 2013), torsional stiffness (Galuppi et al., 2020), and elements undergoing compressive buckling (D’Ambrosio et al.,

2020). The EET equations are here reformatted, showing that they can take a common form for 1-dimensional (beam) bending and torsion. This may be done by introducing a term K, defined in this paper for each of the characteristic stiffnesses being analyzed. Some formulas and derivations from the papers mentioned above for bending are included for completeness.

## 4.2. Elastic Buckling Formulas for Unrestrained Cantilevers

The most commonly applied formula for cantilever glass fins is from AS1288 Appendix C, which is of the form:

$$M_{CR} = (g_2/L_{ay})[(EI)_y(GJ)]^{\frac{1}{2}} \left\{ 1 - g_3 \left( \frac{y_h}{L_{ay}} \right) [(EI)_y/(GJ)]^{1/2} \right\} \quad (4)$$

(Note that the division sign is missing between the EI/GJ terms in the 2021 printing of AS 1288)

Table 2: Comparison of stability factors.

| Loading                                | Slenderness factors (AS1288) |                        | Slenderness factors (converted EU) |       |
|--|------------------------------|------------------------|------------------------------------|-------|
|  | $g_2$                        | $g_3$                  | $C_1$                              | $C_2$ |
| for a point load on the cantilever     | 4.0                          | 2.0<br>(Corrected 1.0) | 1.25                               | 0.318 |
| For a distributed load on a cantilever | 6.4                          | 2.0                    | 2.037*                             | 0.637 |

\*AS4100 suggests 2.25 for loads applied at the centroid.

However, the line for the point load on a cantilever is contradicted by Timoshenko and Gere which states:

$$P_{CR} = \frac{4.013\sqrt{EI\eta C}}{l^2} \left( 1 - \frac{a}{l} \sqrt{\frac{EI\eta}{C}} \right) \quad (5)$$

Where  $C = GJ$  and  $a$  is the height of the point load above the centroid.

Noting that  $M_{CR} = P_{CR} * l$ , we can see that the  $g_3$  term for a point load should be 1. Finite element modelling spot checks confirms that the Timoshenko and Gere presentation is the correct one.

For a distributed load Timoshenko and Gere only present the case for the load at the centroid.

$$(ql)_{CR} = \frac{12.85\sqrt{EI\eta C}}{l^2} \quad (6)$$

Noting that  $M_{CR} = (ql)_{CR} * l/2$ , we can see a direct correlation and the  $g_3$  factor appears to behave sufficiently accurately in spot checks.

For comparison to the equation of the format in (2), moving one of the  $\pi$  terms into the brackets,

$$M_{CR} = C_1 \cdot \frac{(\pi E_g I_y)}{L^2} \cdot \left[ \sqrt{(C_2 \pi y_a)^2 + \frac{(G_g J L^2)}{E_g I_y}} - C_2 \pi y_a \right] \quad (7)$$

And noting that it can be demonstrated that  $(C_2\pi y_a)^2$  is small relative to  $\frac{(G_g J L^2)}{E_g I_y}$ , then the forms of the stability equations can be related by  $g_2 = C_1\pi$  and  $g_3 = C_2\pi$ . As  $C_1$  also relates to the moment modification factor relative a beam with constant moment (also referred to as  $C_b$  in AISC 360 and the Aluminum Design Manual and  $\alpha_m$  in AS4100), the format in (2) is now more customary, it is presented in further formulations.

NASA document N.A.C.A Technical Note No 601 (Dumont, 1937) presents the factor K which is the same as “ $g_2$ ” in AS1288 and  $C_1*\pi$ , in the customary European formatting for solid rectangular beams. (Note K’ is a similar relation to buckling stress and is not related to  $g_3$ .)

N.A.C.A. Technical Note No. 601 25

TABLE I  
CONSTANTS FOR DETERMINING THE LATERAL STABILITY OF SOLID DEEP RECTANGULAR BEAMS

| CASE | SIDE VIEW | TOP VIEW | K     | K'   |
|------|-----------|----------|-------|------|
| 1    |           |          | 3.14  | 1.86 |
| 2    |           |          | 6.28  | 3.71 |
| 3    |           |          | 6.28  | 3.71 |
| 4    |           |          | 9.22  | 5.45 |
| 5    |           |          | 3.54  | 2.09 |
| 6    |           |          | 6.10  | 3.61 |
| 7    |           |          | 8.24  | 4.87 |
| 8    |           |          | 4.235 | 2.50 |
| 9    |           |          | 6.47  | 3.82 |
| 10   |           |          | 11.12 | 6.57 |
| 11   |           |          | 13.1  | 7.74 |
| 12   |           |          | 5.29  | 3.13 |
| 13   |           |          | 5.88  | 3.48 |
| 14   |           |          | 4.01  | 2.37 |
| 15   |           |          | 4.01  | 2.37 |
| 16   |           |          | 6.43  | 3.80 |
| 17   |           |          | 6.43  | 3.80 |

Fig. 1: Stability coefficients for various boundary conditions.



For glass design, the more common usage is to cantilever glass fins from the ceiling with a combination of point load at the tip and distributed load on the length. In this instance the load is restrained laterally which strongly influences the stability. Here the work by Trahair incorporated in AS 4100 is particularly useful and as the load mechanism provides restraint and cannot move laterally, the  $C_2$  (and hence also  $g_3$ ) terms should be considered to be zero.

Table 3 Cantilever stability coefficients

| Loading  | Slenderness factors<br>(AS1288) |       | Slenderness factors<br>(converted EU) |       |
|--|---------------------------------|-------|---------------------------------------|-------|
|  | $g_2$                           | $g_3$ | $C_1$                                 | $C_2$ |
| For a point load on the cantilever with end restrained | 5.5                             | -     | 1.75                                  | -     |
| For a distributed load on a cantilever                 | 11                              | -     | 3.5                                   | -     |

While spot checks for UDL of AS1288 for distributed load on cantilevers appears to have reasonable agreement, SN006a-EN-EU suggests a more complex interaction with  $g_3$ , or suggests  $g_3 = 0$  for  $I_{ww} = 0$ . Nethercott and Rockney also suggest  $g_3=0$ . While the warping coefficient,  $I_{ww}$  is often ignored for glass fins due to the slenderness ratio, it is not zero. It is also worth noting for laminated glass fins the assumption of thin-walled sections where the Saint-Venant torsion constant  $J = b.t^3/3$  can be non-conservative. Comparison of different methods as a function of  $I_{ww}$  is well presented in depth by Kraus, Crisan and Wittor (2021) in *Stability Study of Cantilever-Beams – Numerical Analysis and Analytical Calculation (LTB)*. To make better use of the table in NCCI it is important to have accurate torsional properties.

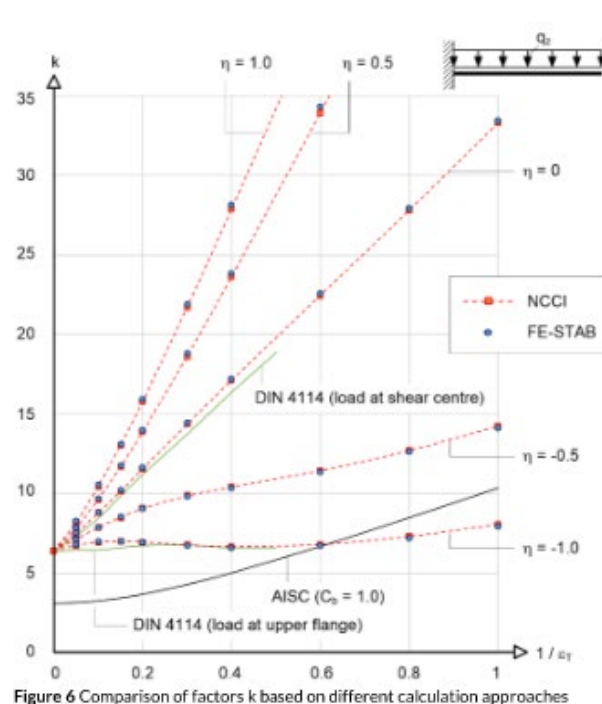


Fig. 2: Comparison of cantilever stability approaches, from Kraus, Crisan and Wittor (2021).

### 4.3. Torsion Constants for Rectangular Shapes

The Saint Venant torsion constant in the most accurate form is an infinite series.

$$J = \frac{1}{3} a^3 b \left( 1 - \frac{192 a}{\pi^5 b} \sum_{n=1,3,5}^{\infty} \frac{1}{n^5} \tanh \frac{n\pi b}{2a} \right) \quad (8)$$

where: a is the minor dimension and b is the major dimension.

There are a variety of simplifications: the simplest and most common is “thin-walled” approximation for  $a \ll b$

$$J = \frac{1}{3} a^3 b \quad (9)$$

The version in AS 1288 is:

$$J = \frac{1}{3} a^3 b \left( 1 - 0.63 \left( \frac{a}{b} \right) \right) \quad (10)$$

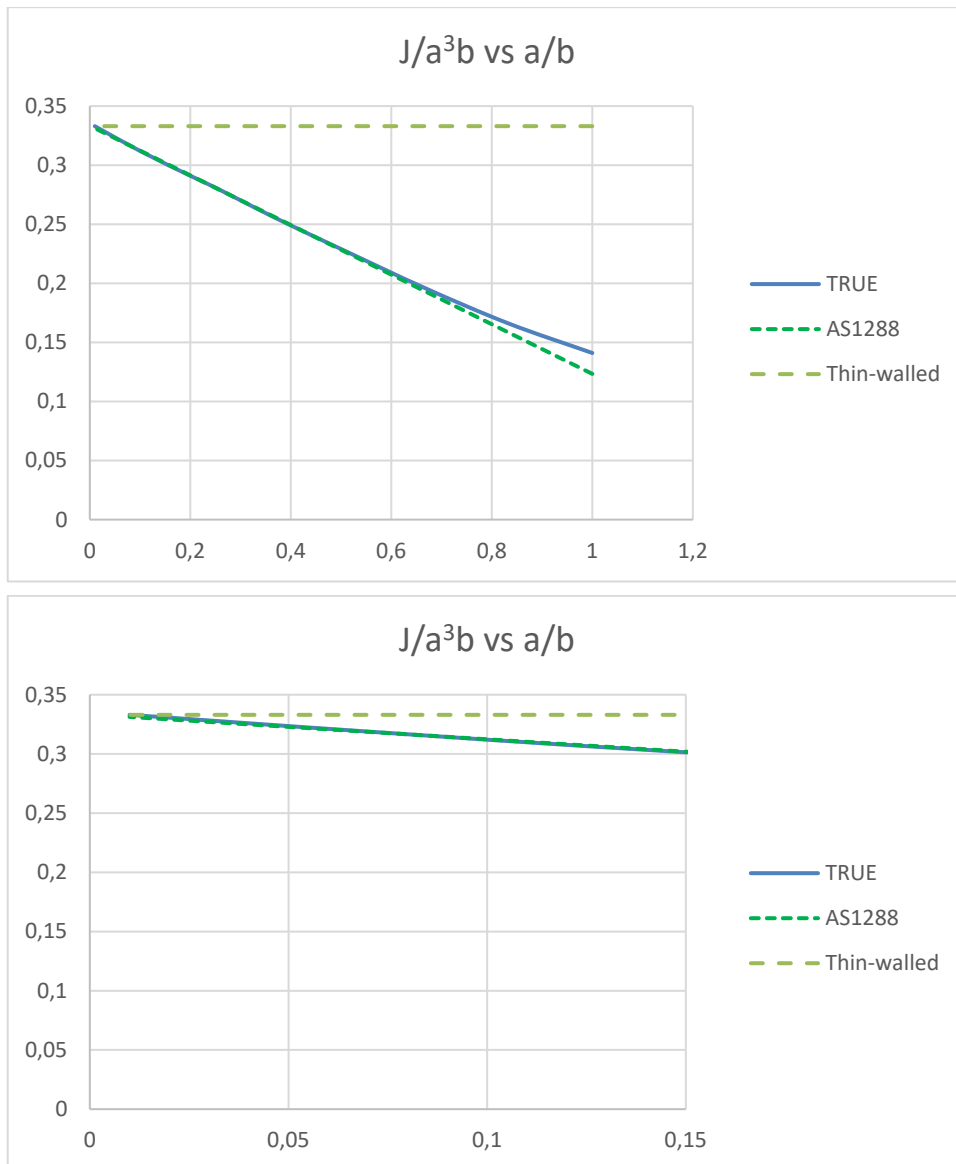


Fig. 3a & 3b: Comparison of torsion constant ( $J$ ) formulations.

For monolithic fins with common aspect ratios of 20:1 ( $a/b = 0.05$ ) the thin-walled is still valid, however for laminated assemblies of greater thickness the deviation may become significant, in which case the version in AS 1288 is adequately accurate (<0.5% deviation) for aspect ratios of 2:1 or greater.

For the warping constant, the authors were unable to find a closed form solution for rectangles of non-negligible thickness. For I beams, where the thickness of the flange is small relative to the separation of the flange centroid from the shear center,  $I_{ww}$  is well defined by using the centerline approximation where

$$I_{ww} \cong \sum I_{y,fl} \cdot \hat{y}_{fl}^2 \cong \frac{I_y \cdot d_{fl}^2}{4} \quad (11)$$

Where  $\hat{y}_{fl}$  is the distance from the centroid of the flange of the I-beam from the shear center and  $d_{fl}$  is the distance between the centroids of the flanges (or the height of the beam less a flange thickness) This approach is also valid for the layered state laminated assembly with the assumption that all plies rotate about a common shear center.

For rectangular sections the relationship between  $I_{ww}$  is more complex and as the section becomes more square, symmetry dictates that all corners have to have the same warping function, hence must be zero. The authors were unable find a closed form solution for  $I_{ww}$ , however by conducting multiple calculations using the membrane analogy, calculation of  $I_{ww}$  in the section property of Strand7 (Strauss 7 in Europe), a suitable curve fit can be formed.

$$I_{ww} = \frac{B^3 D^3}{144} [1 - (2.4649 x^4 - 6.9103 x^3 + 5.4827 x^2 - 0.0567 x)] \quad (12)$$

where  $x = a/b$ ,  $a$  is the minor dimension and  $b$  is the major dimension.

The above equation has an error less than 1% across the range.

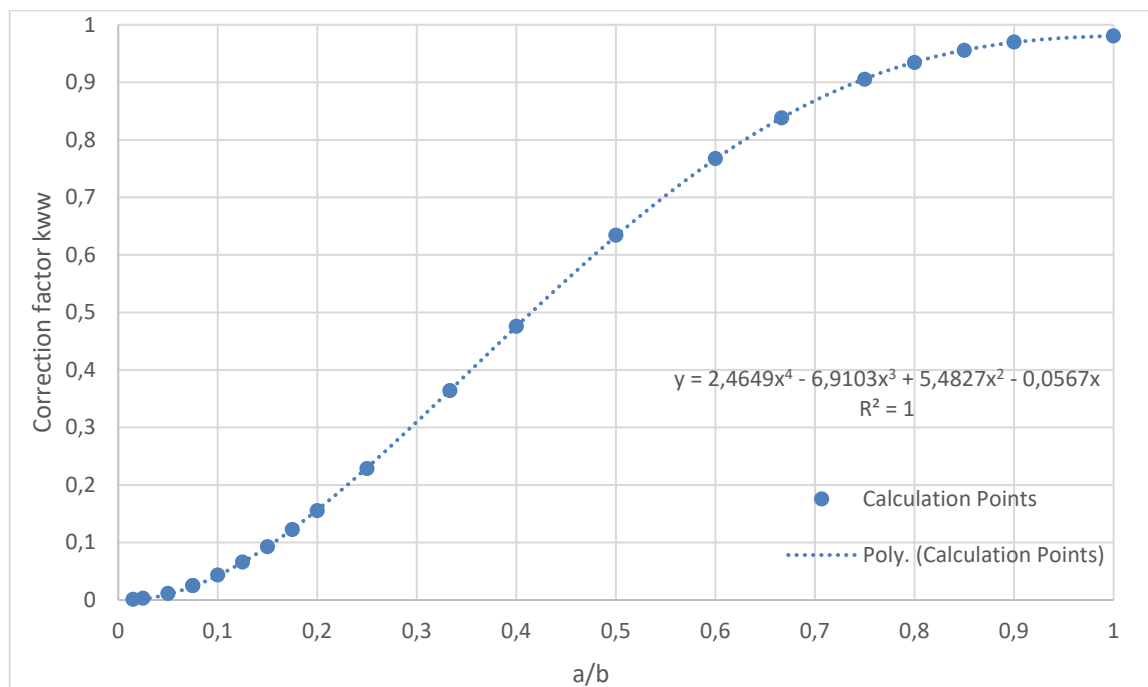


Fig. 4: Correction Factor  $k_{ww}$  vs  $a/b$ , where  $I_{ww} = 1/144 a^3 b^3 (1 - k_{ww})$ .

For most practical glass members with aspect ratios of 5:1 or greater, this is approximated well (<3% error at 5:1 and for 8:1 or greater there is < 1% error).

$$I_{ww} = \frac{B^3 D^3}{144} \left[ 1 - 4.5 \left( \frac{B}{D} \right)^2 \right] \quad (13)$$

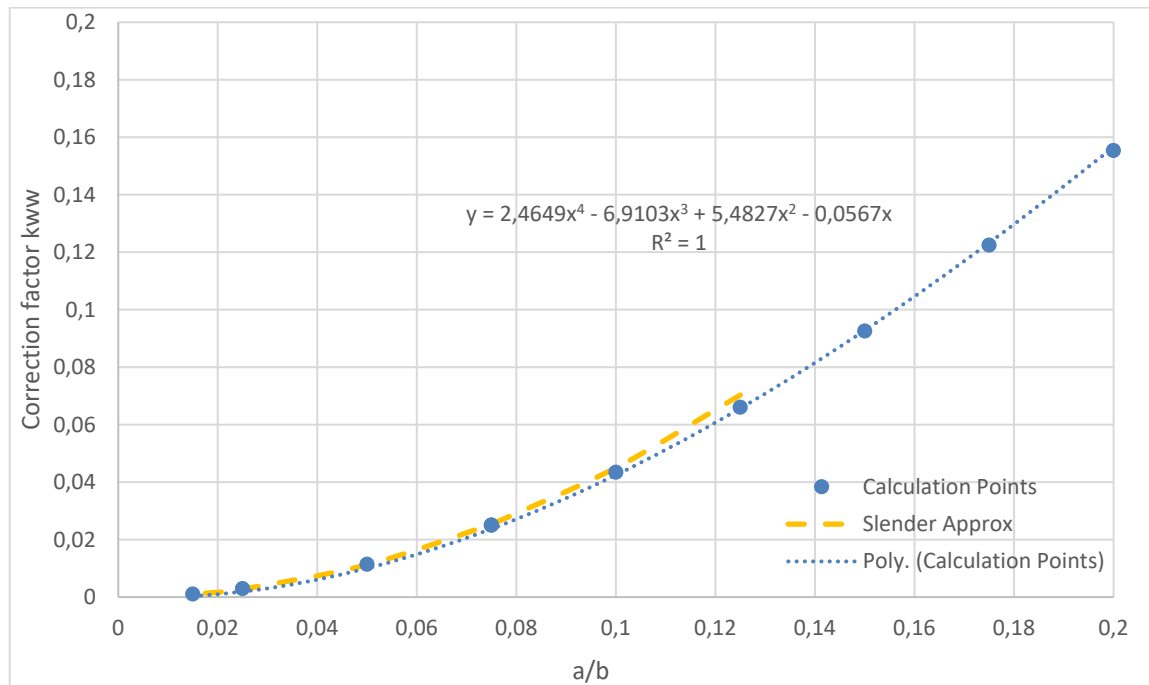


Fig. 5: Simplified  $I_{ww}$  for slender beams.

(Note that the approximation of  $I_{ww} = I_{yy} * D^2 / 4$  that is common for I-beams and is sometimes also applied to rectangles equates to a correction factor of  $48/144 = 0.33$ , so is conservative for warping stiffness for  $a/b < 0.3$ .)

#### 4.4. Summary of Stability Factors for Elastic Critical Buckling

Table 4: Values for C1 and C2 - Beams

| Bending Moment   | Minor axis rotational fixity ( $r_y$ ) | C <sub>1</sub> | C <sub>2</sub> |
|--|--|----------------|----------------|
| Uniform (Constant)                                     | Free                                   | 1              | 0              |
|  | Fixed                                  | 2              | 0              |
| Linear (zero at midspan)                               | Free                                   | 2.7            | 0              |
|  | Fixed                                  |                |                |
| Parabolic (simply supported, zero at both extremities) | Free                                   | 1.127          | 0.454          |
|  | Fixed                                  | 1.942          | 0.573          |
| Parabolic (fixed end)                                  | Free                                   | 1.301          | 1.554          |
|  | Fixed                                  | 1.719          | 1.655          |
| Triangular (central point load, simply supported)      | Free                                   | 1.348          | 0.630          |
|  | Fixed                                  | 2.132          | 0.828          |
| Triangular (central point load, fixed end)             | Free                                   | 1,683          | 1.645          |
|  | Fixed                                  | 2.069          | 1.687          |

For additional coefficients for beams reference: NCCI SN-003-EN-EU

Table 5: Values for C1 and C2 - Cantilevers

| Bending Moment Profile       | Free end lateral fixity (dx) | C <sub>1</sub> | C <sub>2</sub> |
|------------------------------|------------------------------|----------------|----------------|
| Cantilever Point load at end | Free                         | 1.27           | 0.318*         |
|                              | Fixed                        | 1.75           | 0              |
| Cantilever uniform load      | Free                         | 2.040          | 0.637          |
|                              | Fixed                        | 3.500          | 0              |

For additional coefficients for cantilevers reference: NCCI SN-006-EN-EU

NOTES:

For tapered cantilevers further information is available in Timoshenko and Gere (1956)

C1 is the same as  $g2/\pi$  in AS1288 and C2 is the same as  $g3/\pi$  in AS1288.

\* Corrections to coefficients in AS1288 are based on the work of Timoshenko and Gere and as tested against finite element models.

The coefficients for cantilevers with lateral end restraint is based on AS4100 reflecting the work of Trahair.

## 5. Enhanced Effective Thickness (EET) – Bending

Depending on the degree of shear coupling of the glass plies through the interlayer, the out-of-plane bending response of a laminated glass element is intermediate between that of free sliding plies (layered behavior) and that of a glass monolith (monolithic behavior) of the total thickness. In particular, by considering a laminated glass element, of unit width, composed of N glass plies:

- For the *layered behavior*, the moment of inertia with respect to the minor axis is:

$$I'_{plies} = \sum_{i=1}^N I'_i \quad (14)$$

where:  $I'_i = h_i^3/12$  [mm<sup>4</sup>/mm (or in<sup>4</sup>/in)] is the moment of inertia per unit width of the *i*-th glass ply [mm<sup>4</sup>/mm] (notation of Figure 1). (The “prime” mark indicates “per unit width”). Note that, while metric units are presented here, any consistent unit system can be used.

- For the *monolithic limit*, the moment of inertia is:

$$I'_{total} = I'_{plies} + I'_{comp} \quad (15)$$

Where:

$$I'_{comp} = \sum_{i=1}^N h_i d_i^2 \quad (16)$$

and  $d_i$  [mm] is the distance of the centroid of the *i*-th ply from the centroid of the cross-section of the laminated package (Figure 6), while  $h_i$  is the area for a strip of unit width ( $B = 1$ ).

Also,  $A_i = B h_i / 1$  [mm<sup>2</sup>/mm] =  $h_i$  [mm<sup>2</sup>/mm] is the area per unit width of the cross-section of the *i*-th plate, i.e. the ply thickness of the *i*-th ply.

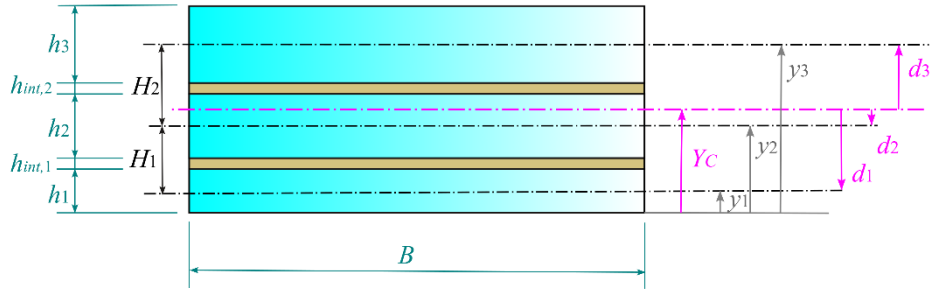


Fig. 6: Geometry of a laminated glass element (cross-sectional view).

In Figure 6,  $h_i (i=1..N)$  is the thickness of the  $i$ -th ply of glass,  $h_{int,i} (i=1..N)$  is the thickness of the  $i$ -th interlayer,  $y_i$  is the position of the centroid of the  $i$ -th ply,  $Y_c$  is the position of the centroid of the glass plies and  $d_i$  is the distance (with sign) from the overall centroid ( $Y_c$ ) to the centroid of the  $i$ -th ply.  $B$  is the width of the assembly.

The distances  $d_i$  may be evaluated as:

$$d_i = y_i - Y_c, \text{ where } Y_c = \frac{\sum_{i=1}^N y_i h_i}{\sum_{i=1}^N h_i} \quad (17)$$

For laminated glass beams, the EET method defines the equivalent moment of inertia as the harmonic mean of the moment of inertia of the cross-section at the monolithic and layered limit, with the harmonic mean weighted using a *shear transfer coefficient*, accounting for the degree of coupling between glass plies due to the presence of the interlayer: For laminated glass beams, the EET method defines the equivalent moment of inertia as the harmonic mean of the moment of inertia of the cross-section at the monolithic and layered limit, with the harmonic mean weighted using a *shear transfer coefficient*, accounting for the degree of coupling between glass plies due to the presence of the interlayer:  $I_{y_{eff}}$  is the effective moment of inertia of the laminated package, assuming an intermediate value between  $I_{total}$  and  $I_{plies}$ .

The effective moment of inertia may be written equivalently as:

$$\frac{1}{I'_{y_{eff}}} = \frac{\eta_b}{I'_{total}} + \frac{1-\eta_b}{I'_{plies}} \quad (18)$$

$$I'_{y_{eff}} = \frac{1}{\left\{ \frac{\eta_b}{I'_{total}} + \frac{1-\eta_b}{I'_{plies}} \right\}} \quad (19)$$

where  $\eta_b$  is a non-dimensional coefficient (suffix b refers to “bending”) depending on the geometry of the beam, on the loading and boundary conditions, and on the mechanical properties of glass and interlayer. The value of  $\eta_b$  ranges from 0 (layered limit) and 1 (monolithic limit).

### 5.1.1. Shear Coupling Coefficient for Beams

The shear coupling coefficient  $\eta_b$  is a function of the geometry of the laminate and the properties of the interlayer (Galuppi et al. 2014)]

$$\eta_b = \frac{1}{1 + \frac{E_g I'_{plies} I'_{comp} \psi}{G_{int} (I'_{total}) K_b}} \quad (20)$$

where:

$E_g$  is the Young's modulus of glass;

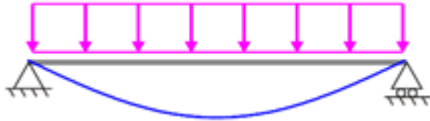

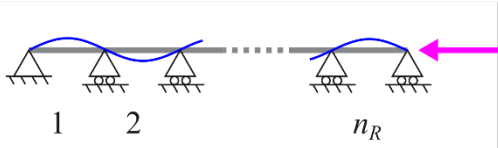
$G_{int}$  is the relaxation shear modulus of the interlayer for the applicable temperature and duration;

$K_b$  is a function of the glass and interlayer geometry defined as:

$$K_b = \sum_{i=1}^{N-1} (y_{i+1} - y_i)^2 / h_{int,i} = \sum_{i=1}^{N-1} H_i^2 / h_{int,i} \quad (21)$$

The coefficient  $\psi$ , appearing in eq. 20, is a function of the beam length  $L$ , the loading profile and the boundary and loading, tabulated in Table 6 for the case of interest. For lateral-torsional buckling\*<sup>1</sup> use  $\pi^2/L^2$ , as in Nizich (2022).

Table 6: Laminated Beams Boundary Conditions: values of coefficient  $\Psi$ .

| Loading and boundary conditions   | $\psi$                    |
|---|---------------------------|
|  | $\frac{168}{17 L^2}$      |
|  | $\frac{\pi^2}{L^2}$       |
|  | $\frac{n_R^2 \pi^2}{L^2}$ |

NOTE: Refer D'Ambrosio et al. (2020) and Galuppi et al. (2013) for different loading and boundary conditions.

\*<sup>1</sup> Note for systems with multiple half-wavelengths, use the distance between points of contraflexure as " $L$ ". For not-restrained laminated glass fins subjected to lateral-torsional buckling, the effective bending inertia  $I_{y_{eff}}$  may be evaluated by using coefficient  $\psi = \pi^2/a^2$ , where  $a$  is the half wave-length, as per Table 6. As  $\psi$  will affect the effective thickness and may change  $n_R$ , the solution may be iterative.

### 5.1.2. Deflection - Effective Thickness for Beams in Bending

The *deflection-effective thickness* is defined as the thickness of the monolithic glass exhibiting the same maximum deflection of the considered laminated glass element under bending. Obviously, the deflection is inversely proportional to the moment of inertia and, therefore, to the cube of the thickness of the equivalent monolith. The deflection-effective thickness is then equal to:

$$\hat{h}_w = \sqrt[3]{12 \cdot I'_{y_{eff}}} \quad (22)$$

### 5.1.3. Stress - Effective Thickness for Beams in Bending

The *stress-effective thickness* is defined as the thickness of monolithic glass exhibiting the same maximum stress in one of the plies of the considered laminated glass element. In general, one defines a stress-effective thickness for each glass ply. The stress-effective thickness of the  $i$ -th plate is given by:

$$\hat{h}_{i;\sigma} = \sqrt{\frac{6}{\frac{\eta_b |d_i|}{I'_{total}} + \frac{h_i}{2 \cdot I'_{y_{eff}}}}} \quad (23)$$

## 5.2. Enhanced Effective Thickness – Torsion\*

### 5.2.1. Effective Torsional Stiffness

Depending on the degree of shear coupling of the glass plies through the interlayer, the torsional response of a laminated glass element is intermediate between that of free sliding plies (layered behavior) and that of a monolith (monolithic behavior) of the total thickness. In particular, for a laminated glass element with unit width, composed of  $N$  plies of glass:

- For the *layered limit*:

$$J'_{plies} = \sum_{i=1}^N J'_i = \frac{1}{3} \sum_{i=1}^N h_i^3 \quad (24)$$

where  $J'_i = h_i^3/3$  [mm<sup>4</sup>/mm] is the torsional moment of inertia of the  $i$ -th glass ply per unit width [mm<sup>4</sup>/mm] and  $B$  is the width of the ply (notation of Figure 1).

- For the *monolithic limit*

$$J'_{total} = J'_{plies} + 4 I'_{comp} \quad (25)$$

$$J'_{total} = \frac{1}{3} \sum_{i=1}^N [h_i^3 + 12 d_i^2 h_i] = \sum_{i=1}^N \left[ \frac{h_i^3}{3} \right] + 4 \sum_{i=1}^N d_i^2 h_i \quad (26)$$

According to the Enhanced Effective Thickness approach for torsion (Galuppi et al., 2020), the effective torsional stiffness of the laminated element may be evaluated by considering:

$$\frac{1}{J'_{eff}} = \frac{\eta_t}{J'_{total}} + \frac{1-\eta_t}{J'_{plies}} \quad (27)$$



$$J'_{eff} = \frac{1}{\left\{ \frac{\eta_t}{J'_{total}} + \frac{1-\eta_t}{J'_{plies}} \right\}} \quad (28)$$

where  $J'_{total}$  is the Saint Venant (uniform) torsional stiffness per unit width at the monolithic limit (defined by eq. (25)); and where  $J'_{plies}$  is the Saint Venant (uniform) torsional stiffness per unit width for the glass plies (defined by eq. (24)). The torsional stiffness of the beam is

$$J_{eff} = J'_{eff} * B \quad (29)$$

where  $B$  is the breadth.

This provides the effective section properties to calculate the critical elastic buckling moment for laminated fins. Notice that the EET method for torsion presented by Galuppi et al. (2020) is based on the thin-walled approximation of  $J_{ply} = \frac{Bh_i^3}{3}$ . However, AS1288 presents a more conservative and accurate version of the formula, that is:

$$J_{ply} = \frac{Bh_i^3}{3} \left( 1 - 0.63 \frac{B}{h_i} \right) \quad (30)$$

Thus, the equivalent term that could be substituted in equation (25) is:

$$J'_{plies} = \frac{1}{3} \sum_{i=1}^N h_i^3 \left( 1 - 0.63 \frac{B}{h_i} \right) \quad (31)$$

If this format is used, it should also be used consistently when back-solving the effective thickness for torsion (35), but that is not presented here because only the torsional stiffness  $J_{ef}$  is used in subsequent equations.

The shear coupling function previously presented by Galuppi et al. (2020) can be rewritten as

$$\eta_t = \frac{1}{1 + \frac{E_g}{(1-\nu^2)G_{int}} \frac{J'_{plies} \cdot I'_{comp}}{J'_{total} \cdot K_t} \psi_t} \quad (32)$$

where:

$$K_t = K_b = \sum_{i=1}^{N-1} H_i^2 / h_{int,i} \quad (33)$$

and

$$\psi_t = 6(1 - \nu) \frac{L^2 + B^2}{L^2 B^2} \quad (34)$$

where  $B$  is the width;  $N$  is the number of glass plies, and  $N-1$  is the number of interlayers.

Notice that the expression (33) for the parameter  $K_t$  coincides with that obtained for the bending problem (eq. 21). This allows for a comprehensive formulation of the EET model, for both bending and torsion, that is proposed here for the first time.

NOTE: This section for effective torsional stiffness is included for stability calculations. For applied torsional loads, the use of layered finite element methods or similar is recommended to capture longitudinal stresses due to warping of each ply, which are not calculated in this method.

### 5.2.2. Effective Thickness for Torsion Deflection

The torsional  $EET \hat{h}_{w;\tau}$  defined as the thickness of a monolithic glass prism of width  $B$  and length  $L$ , having the same geometric torsional constant of the laminated glass element, is given by formula:

$$\hat{h}_{w;\tau} = \sqrt[3]{3 J'_{ef}} \quad (35)$$

If the thick-ply formula from AS1288 presented at equation (31) is substituted at equation (25), then the same equation should be used to iteratively back-calculate the effective thickness for torsion deflection.

### 5.2.3. Effective Thickness for Torsional Stress

The thickness of a monolith for which the maximum shear stress in the  $i$ -th glass ply equals the maximum shear stress in glass for the laminated package is:

$$\hat{h}_{i;\tau} = \sqrt{\frac{\hat{h}_w^3}{h_i + \alpha |d_i|}} \quad (36)$$

$$\alpha = \frac{2}{1 + \frac{E}{(1-\nu^2)G_{int}} \frac{\sum_{i=1}^N h_i d_i^2}{\sum_{i=1}^{N-1} H_i^2 / h_{int,i}}} \psi_t = \frac{2}{1 + \frac{E}{(1-\nu^2)G_{int}} \frac{I_{comp}}{K_t}} \psi_t \quad (37)$$

## 5.3. Continuously Elastically Restrained Fins

Bedon et al. (2015) proposes the equations for fins with continuous elastic lateral restraint under uniform moment in the following form: (notation altered for US customary axis system, where “z” is the longitudinal axis - see Glossary.)

### 5.3.1. Compression Flange Continuously Restrained by a Spring

For fins continuously restrained on the compression flange by a (distributed) spring (Bedon et al., 2015), as shown in Figure 3, the critical buckling moment can be evaluated as:

$$M_{cr,R} = y_m k_x \left(\frac{L}{n_R \pi}\right)^2 + \sqrt{\left[ E_g I_y \left(\frac{n_R \pi}{L}\right)^2 + k_x \left(\frac{L}{n_R \pi}\right)^2 \right] \left[ G_g J + y_m^2 k_x \left(\frac{L}{n_R \pi}\right)^2 \right]} \quad (38)$$

where

- $y_m$  is the height of the spring above the shear center (positive on the compression flange side);
- $k_x$  is the stiffness of the spring per unit length;
- $n_R$  is the number of half wavelengths of the buckled mode;  $n_R$  is an integer, try different values for  $n_R$  and use the minimum value for  $M_{cr,R}$ ;
- when calculating the effective properties for laminated glass, the composite action development length shall not exceed the half wave-length ' $a' = L/n_R$ '

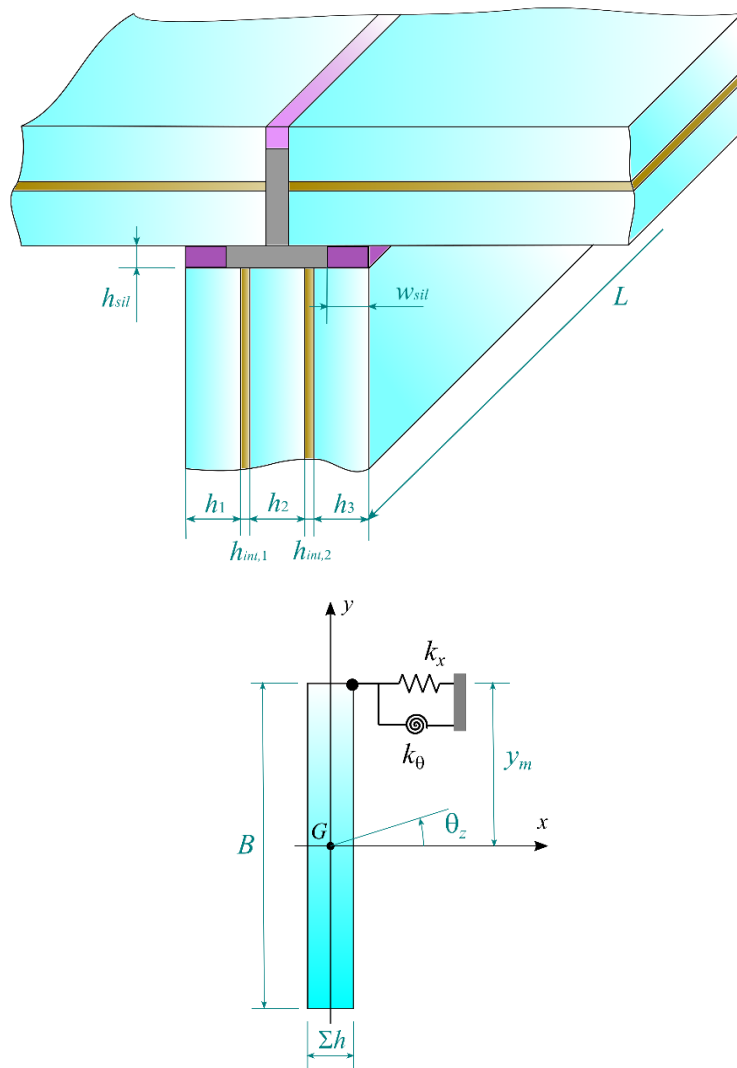


Fig. 7: Typical façade glass to beam connection by means of continuous silicone joints. (a) Overview and (b) analytical model (cross-section). Figure adapted from Bedon et al. (2015) and revised for US sign conventions.

Notice that only the lateral stiffness of the silicone between the beam and façade glass is included in the derivation, the torsional resistance is not included, and the weather seal between the façade glass is not assumed to participate. If there is more than one piece of façade glass along the length of the beam, the stiffness of the façade glass to restrain the beam should be assessed separately, similar to springs in series.

Notice that the C2 terms, appearing in eq.s (1) and (2) for the case of unrestrained beam, related to load position, does not appear in this formulation. This is because the load is restrained from moving laterally.

### 5.3.2. Tension Flange Continuously Restrained by a Spring

Bedon et al. (2015) also develops a form for “reverse moment” with continuous elastic restraint of the tension flange:

$$M_{cr,R} = y_m k_x \left( \frac{L}{n_R \pi} \right)^2 - \sqrt{\left[ E_g I_y \left( \frac{n_R \pi}{L} \right)^2 + k_x \left( \frac{L}{n_R \pi} \right)^2 \right] \left[ G_g J + y_m^2 k_x \left( \frac{L}{n_R \pi} \right)^2 \right]} \quad (39)$$

where the input terms are as defined above.

### 5.3.3. Combined Equation

The above equations (27) and (28) can be efficiently consolidated into a single equation:

$$M_{cr,R} = \sqrt{\left[ E_g I_y \left( \frac{n_R \pi}{L} \right)^2 + k_x \left( \frac{L}{n_R \pi} \right)^2 \right] \left[ G_g J + y_m^2 k_x \left( \frac{L}{n_R \pi} \right)^2 \right]} + y_m k_x \left( \frac{L}{n_R \pi} \right)^2 \quad (40)$$

where the term  $y_m$  is positive for restraint on the compression side of the beam and  $y_m$  is negative for the reverse moment case or where the restraint is on the tensile side of the beam.

Note that substituting in  $n_R = 1$  and  $y_m = 0$ , Eq. (40) reduces to the same classical equation of critical buckling moment of an unrestrained beam (1 half wavelength) under uniform moment. When substituting a large value for  $k_x$ , Eq. (40) also approaches the results for continuously restrained fins in AS1288, which is believed to have originated with timber beams nailed to sheathing, i.e. it ignores the flexibility of the silicone.

In Bedon's paper, it is suggested that capacity modification factor factors can be applied for non-uniform moment profiles in the same manner as an unrestrained beam, however in benchmarking it is the moment profile over the critical half-wavelength (similar to local buckling) that is relevant for accurate prediction of the elastic buckling moment. For simply supported beams under uniform load, for  $n_R \geq 3$  the moment over the critical segment is sufficiently uniform for it to be of limited benefit. Using the formula for  $C_b$  in AISI 360 and parabolic moment profile yields the correction factors in Table 7, which can be used in place of  $C_I$  in equations (41) and (42).

Table 7: Capacity modification factor,  $C_b$ , as a function of number of half-wave lengths for a simply supported beam with uniformly distributed load.

| $n_R$ | 1     | 2     | 3     | 4     | 5     | 6     |
|-------|-------|-------|-------|-------|-------|-------|
| $C_b$ | 1.136 | 1.299 | 1.014 | 1.061 | 1.005 | 1.026 |

### 5.4. Laminated Beams Continuously Restrained by a Spring

For laminated beams with non-uniform moment this becomes:

$$M_{cr,R,lam} = C_1 \sqrt{\left[ E_g I_{y_{eff}} \left( \frac{n_R \pi}{L} \right)^2 + k_x \left( \frac{L}{n_R \pi} \right)^2 \right] \left[ G_g J_{eff} + y_m^2 k_x \left( \frac{L}{n_R \pi} \right)^2 \right]} + y_m k_x \left( \frac{L}{n_R \pi} \right)^2 \quad (41)$$

Where, again,  $y_m > 0$  for restraint on the compression side, and  $y_m < 0$  for the "reverse moment" case or where the restraint is on the tensile side of the beam and  $C_I$  is a function of the moment profile in the critical half-wave. (See also table 7)

Because the differential shear between the plies that mobilizes the interlayer under curvature reverses direction at the point of contra-flexure of the beam, the length parameter must be taken as the half-wavelength, not the full length of the beam when calculating the enhanced effective thickness properties. This means that  $I_{y_{eff}}$  is evaluated, by means of the EET method, by using coefficient  $\psi = \pi^2 / a^2$ , where  $a$  is the half wave-length, as per Table 2, and  $a = L / n_R$ .

Using the same spreadsheet for both the effective section properties and the critical moment allows rapid testing of different  $n_R$  values in order to find the respective effective section properties and the critical elastic buckling moment.

For systems which have a relatively short half-wave length and high  $n_R$ , the effective St Venant torsional stiffness can become small and the warping stiffness can become appreciable. In this case, an expanded form of the equation including the warping constant is proposed:

$$M_{crR,lam,I_w} = C_1 \sqrt{\left[ E_g I_{y_{eff}} \left( \frac{n_R \pi}{L} \right)^2 + k_x \left( \frac{L}{n_R \pi} \right)^2 \right] \left[ E_g I_w \left( \frac{L}{n_R \pi} \right)^2 + G_g J_{eff} + y_m^2 k_x \left( \frac{L}{n_R \pi} \right)^2 \right]} + y_m k_x \left( \frac{L}{n_R \pi} \right)^2 \quad (42)$$

This case then raises the question of how to calculate the warping constant  $I_w$  for a laminated fin. While solid rectangles have a non-zero warping constant, the authors are not aware of a formula for their calculations for laminated elements. For the fully composite state, finite element solutions, such as the beam section generator in Strand7 (Strauss7 in Europe) may be used.

The warping constant for the layered state is well approximated by the warping function of the centerlines of the plies. Similar to the warping constant of an I-beam, the warping constant of symmetric layered fins is:

$$I_{w,plies} \cong \sum_{i=1}^n d_i^2 \frac{h_i B^3}{12} \quad (43)$$

For non-symmetric laminates it is required to solve the fundamental equations with the net axial thrust of each ply being zero, to give the additional equations to be able to solve the matrix for the shear center. That is not covered in this paper and evaluation by numerical methods is a more accurate alternative.

For the cases tested at the time of writing, the interpolation function has not been fully developed, however noting that:

- both the layered and the solid have warping constants of similar magnitude;
- both Saint-Venant torsion and warping constants are dominated by shear across the width of the section;
- the effect of the warping constant is relatively small, so some inaccuracy will have a small influence in the overall result;
- it is suggested that using the interpolation function for Saint Venant torsion may be sufficiently accurate until a better option is developed. (Note for very critical cases, confirmation by testing and layered finite element models is recommended.)

$$I_{w_{ef}} \cong \frac{1}{\left\{ \frac{\eta_t}{I_{w,total}} + \frac{1-\eta_t}{I_{w,plies}} \right\}} \quad (44)$$

## 5.5. Spring Stiffness

Typically, the spring is structural silicone to the façade glass. Where the façade glass is a single piece of glass that is fixed laterally, the spring is well approximated by the stiffness of the silicone. For shear stiffness, the constitutive response is approximately linear.

The local spring stiffness per unit length can be calculated as:

$$k_x = G_{ss} \cdot \sum w_{sil} / h_{sil} \quad (45)$$

where:

$G_{ss}$  is the shear stiffness of the structural silicone;

$\sum w_{sil}$  is the total bite of the silicone;

$h_{sil}$  is the glue-line thickness of the silicone (See also Figure 7).

### 5.5.1. Multiple Facade Glass Panels

The above formula is for the spring stiffness between the fin and facade glass that braces it. Where there are multiple pieces of façade glass along the length, the flexibility of the support from the façade glass needs to be considered in the spring constant. (Similar to springs in series reducing the apparent stiffness.)

### 5.5.2. Spring Stiffness of a Silicone Bite in Tension/Compression

In this configuration, the stiffness is non-linear. It is suggested to consult with the manufacturer for suitable values. However, it is conservative to use a lower bound approximation of the stiffness.

## 6. Imperfect Beams

With the effective section properties and critical elastic buckling moment, the capacity can be calculated by considering the initial imperfections. As the critical buckling moment is approached, the second-order effects become significant in calculating the total tensile stress that limits the capacity of the beam.

The Kala equation for imperfect beams (Kala, 2013) provides a method for including the second order effects as a function of target stress level, the level of imperfection, section properties, and the elastic critical buckling moment.

$$M_n = -\frac{\sqrt{4D_1^2 + (D_4 + D_5)^2 + 4D_1(D_4 - 2M_{cr}^* D_3)}}{4M_{cr}^* S_y} + \frac{2D_1 + D_4 + D_5}{4M_{cr}^* S_y} \quad (46)$$

with:

$$D_1 = f'_g M_{cr}^* S_x S_y$$

$$D_2 = M_{cr}^* S_y + N_{cry} |a_{u0}| S_x$$

$$D_3 = M_{cr}^* S_y - N_{cry} |a_{u0}| S_x$$

$$D_4 = 2N_{cry}^2 I_x |a_{u0}|$$

$$D_5 = 2M_{cr}^* D_2$$

$$N_{cry} = \pi^2 \frac{E_g I_y}{L^2}$$

where:

$I_x$  is the second moment of area about the X axis (strong axis);

$I_y$  ( $I_{y_{eff}}$  for laminated sections) is the (effective) second moment of area about the Y axis (weak axis);

$S_x$  is the elastic section modulus about the X axis (strong axis);

$S_y$  is the (effective) elastic section modulus about the Y axis (weak axis), for laminated glass use

$$S_{y_{eff}} = \hat{h}_{i,\sigma;min}^2 / 6 \quad (47)$$

where:

$\hat{h}_{i,\sigma;min}$  is the minimum stress-effective thickness, evaluated according to eq. (23).

$F'_g$  is the glass design tensile strength (i.e. the target stress for a given level of reliability);

For the purpose of  $N_{cry}$  (appearing in the definition of  $D_2$ ,  $D_3$  and  $D_4$ ),  $L$  is the overall length of the beam, **not** the half-wave length, because the unrestrained flange will buckle in a single half-wave ( $L$ ) in the critical case (assuming no torsional restraint from the silicone). For laminated glass beams,  $N_{cry}$  may be evaluated by adopting the EET approach (see Sect. 2.2), with  $\psi = \frac{\pi^2}{L^2}$ , or by adopting other models proposed by the literature [15]. Note that  $\psi$  for weak axis beam bending stiffness is  $\frac{168}{17L^2} = \frac{9.882}{L^2}$ , is only a 1.3% difference to  $\psi = \frac{\pi^2}{L^2} = \frac{9.870}{L^2}$  for axial buckling. The difference in effective stiffness is even smaller and, for simplicity and allowing for the non-uniform compression along the beam, the more conservative beam value was used in the numerical comparison in section 4 below.

As the imperfection parameter  $a_{uo}$  needs to capture the maximum of the torsional imperfection, lateral imperfection or combination thereof, the following definitions are proposed to capture the worst case. The maximum assumed design imperfection,  $a_{uo}$ , is measured perpendicular to the Y axis as defined below in figure 3:

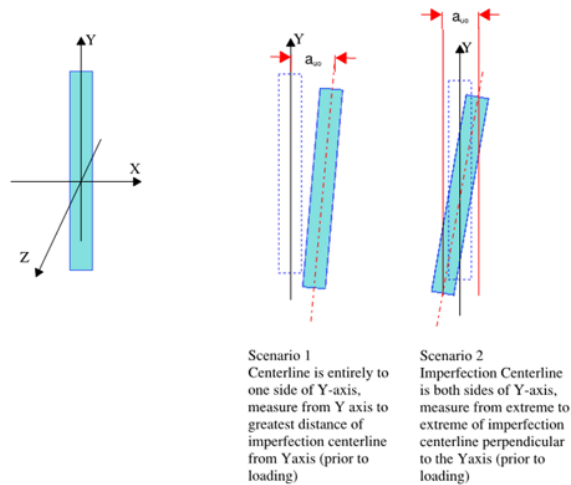


Fig. 8: Imperfect Beams' Characteristic Dimension,  $a_{u0}$ .

NOTE: At the time of writing it has been noted that due to the high slenderness of glass fins, with large differences between  $I_x$  and  $I_y$ , that for unrestrained beams it is important to consider application of loads to the principal axes with the associated minor axis bending stress. However in the context of a continuously restrained beam, the formulation previously stated by Kala is acceptable with suitable reductions as suggested below.

### 6.1. Parametric Analysis

For this case of a theoretical 6 m beam with breadth of 450 mm, and a construction of 9.02 mm+1.52 mm+9.02 mm laminated glass (ASTM minimum thickness for 3/8" (10mm) glass), the interlayer having a stiffness of 3 MPa, with 2 structural silicone bites of 6 mm and an 8 mm glue-line which have a shear modulus of 0.3 MPa, and an initial imperfection of 12 mm ( $L/500$ ), figure 4 shows the nominal moment design capacity, for both tension and compression edges, as a function of the glass design stress.

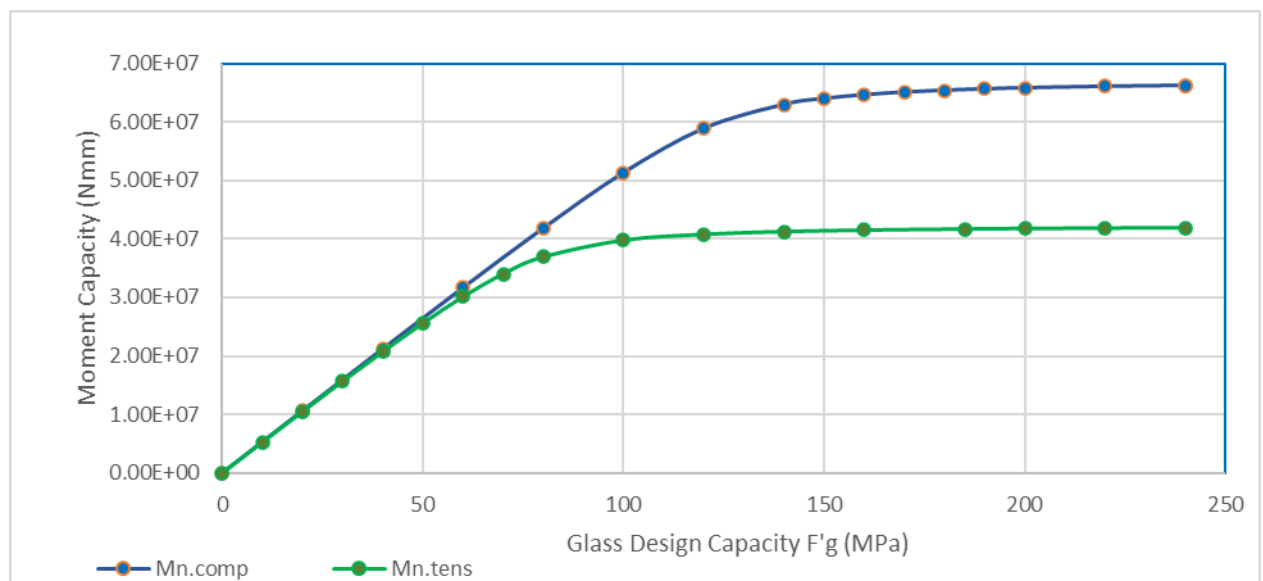


Fig. 9: Nominal Moment Capacity vs Glass Design Capacity ( $F'_g$ ) for beams with continuous elastic restraint to compression edge (Mn.comp) and tension edge (Mn.tens).



Figures 10a-f are for the same scenario described above for figure 9 with nominated input parameters varied.

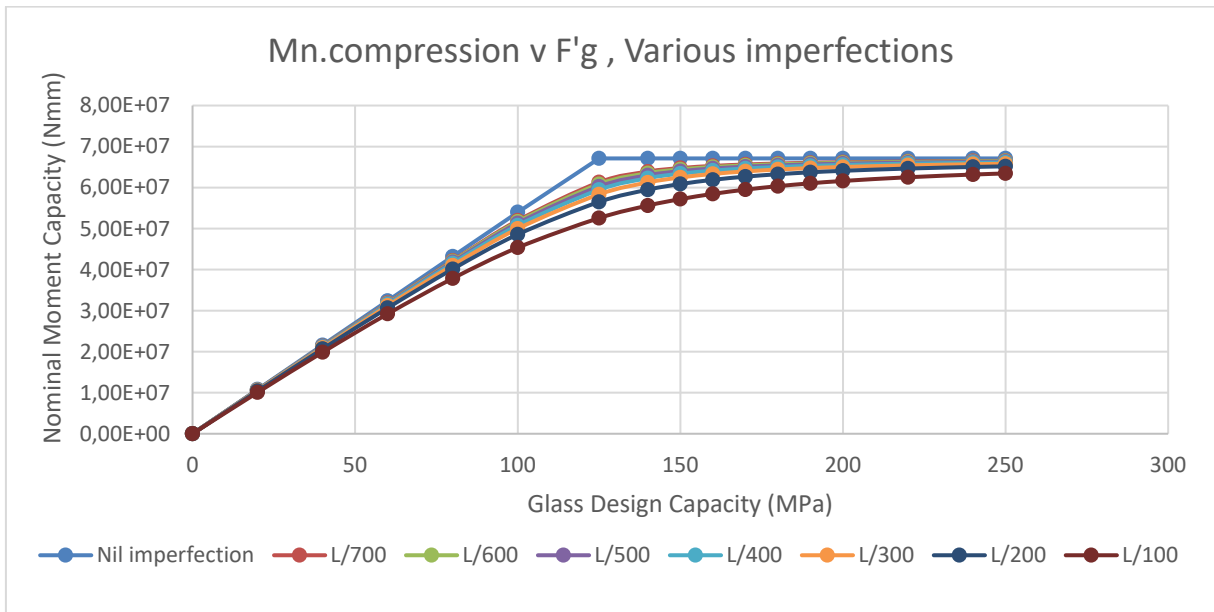


Fig. 10a. Nominal Moment Capacity (Nmm) with compression edge restrained vs Glass Design Capacity (F'g) (MPa), for different values of the initial imperfection.

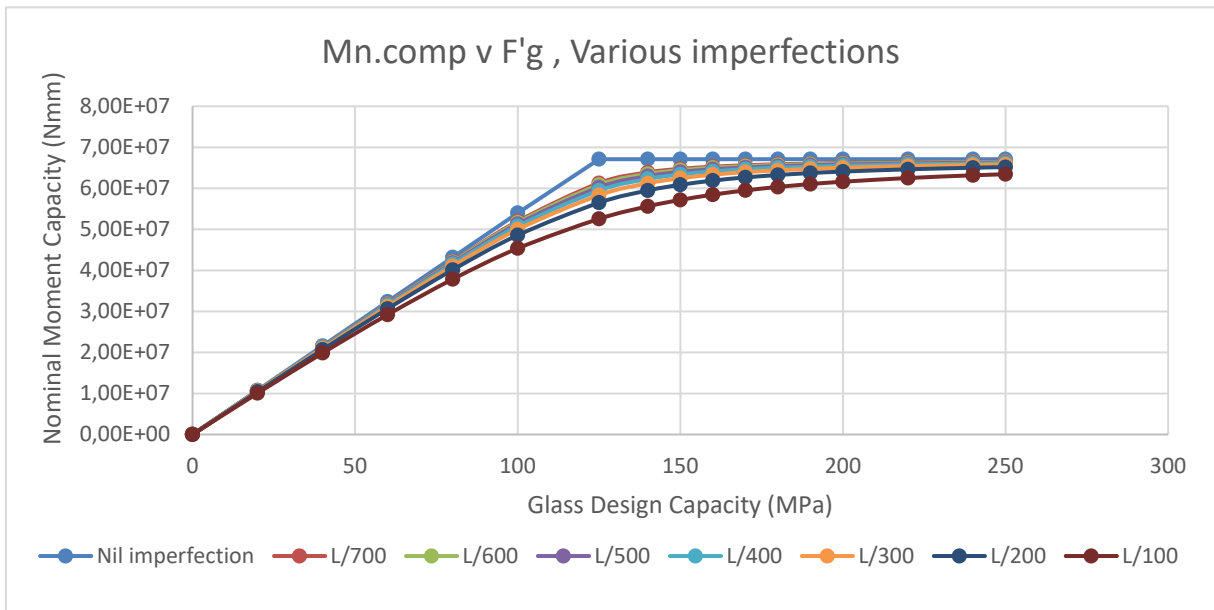


Fig. 10b: Nominal Moment Capacity (Nmm) with tension edge restrained vs Glass Design Capacity (F'g) (MPa), for different values of the initial imperfection.

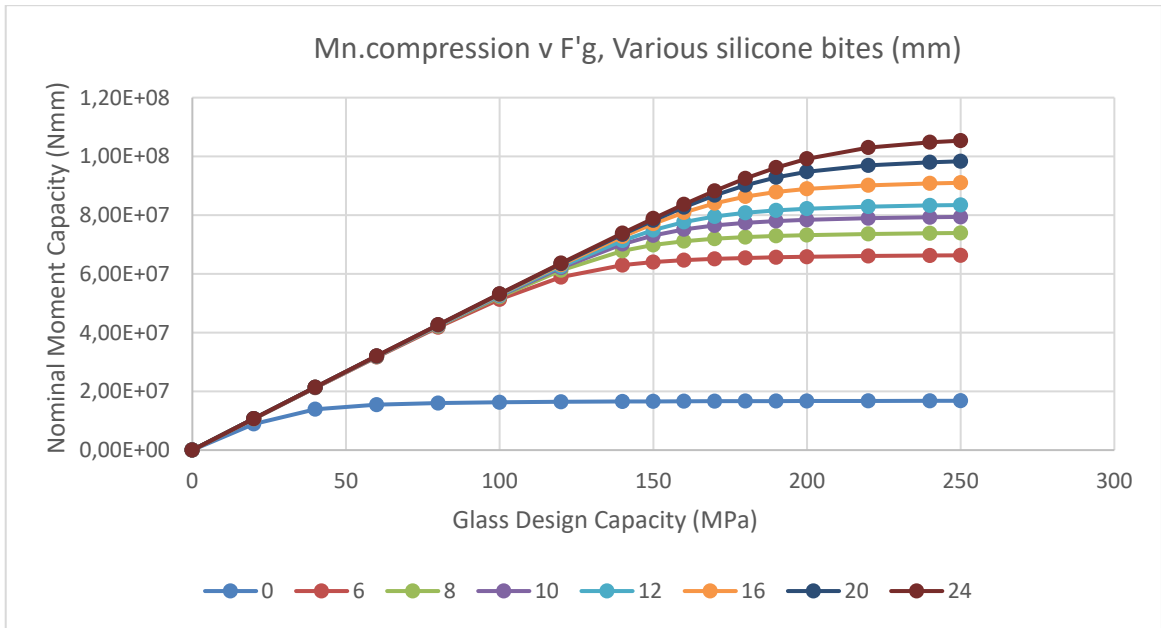


Fig. 10c: Nominal Moment Capacity (Nmm) with compression edge restrained vs Glass Design Capacity ( $F'g$ ) (MPa), for different thickness of the silicone bite (mm).

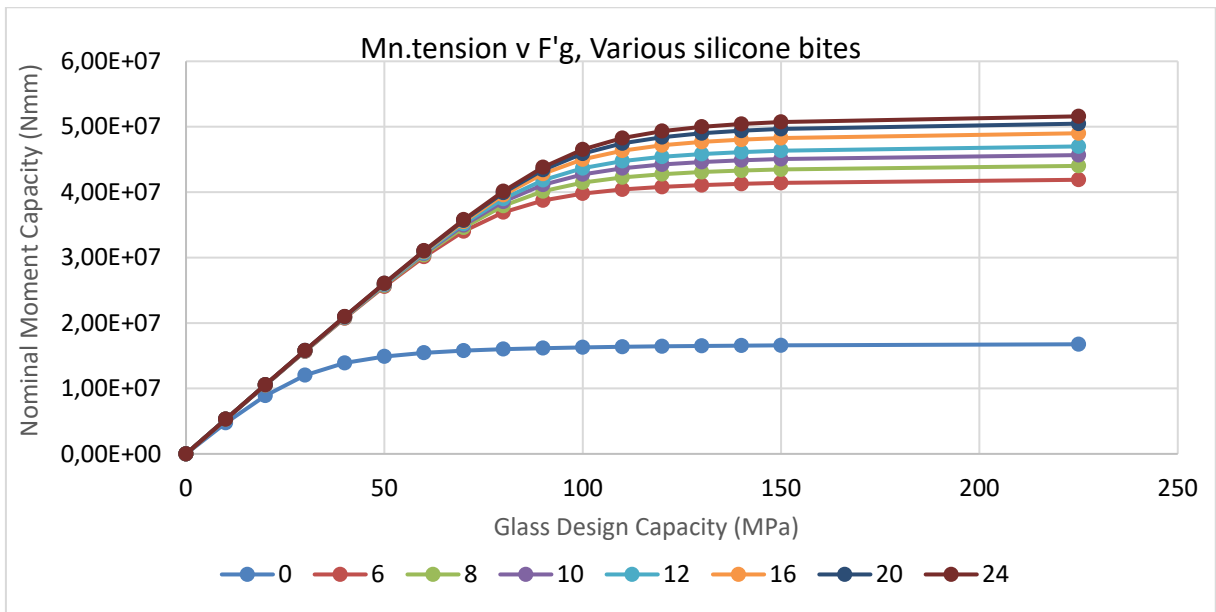


Fig. 10d: Nominal Moment Capacity (Nmm) with tension edge restrained vs Glass Design Capacity ( $F'g$ ) (MPa), for different thickness of the silicone bite (mm).

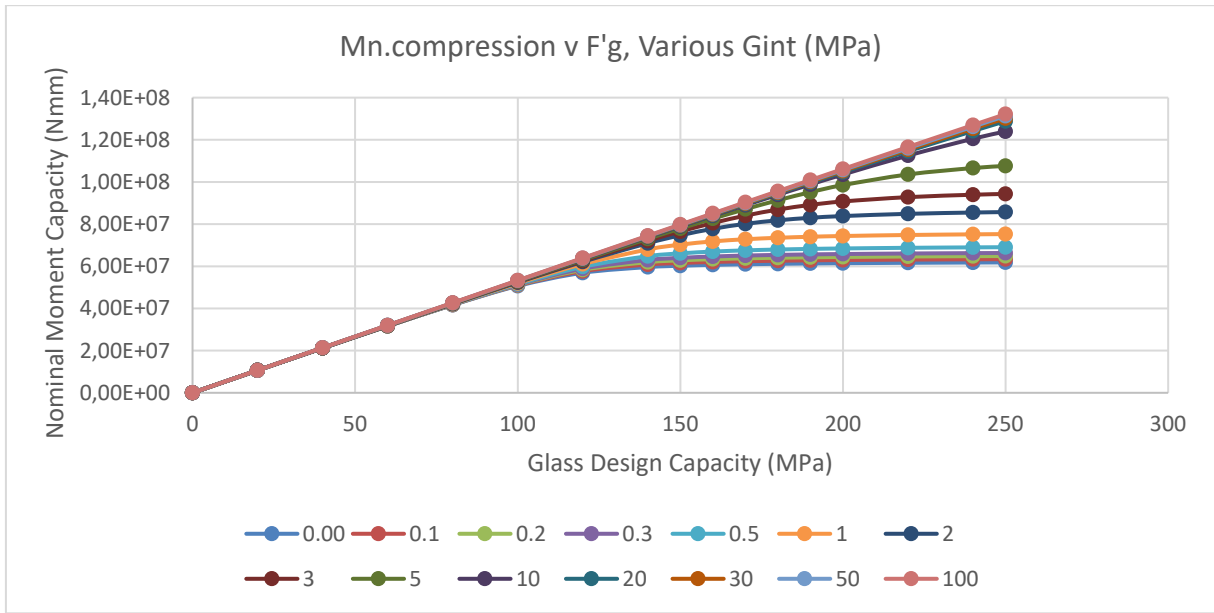


Fig. 10e: Nominal Moment Capacity (Nmm) with compression edge restrained vs Glass Design Capacity ( $F'g$ ) (MPa), for different shear moduli of the interlayer (MPa).

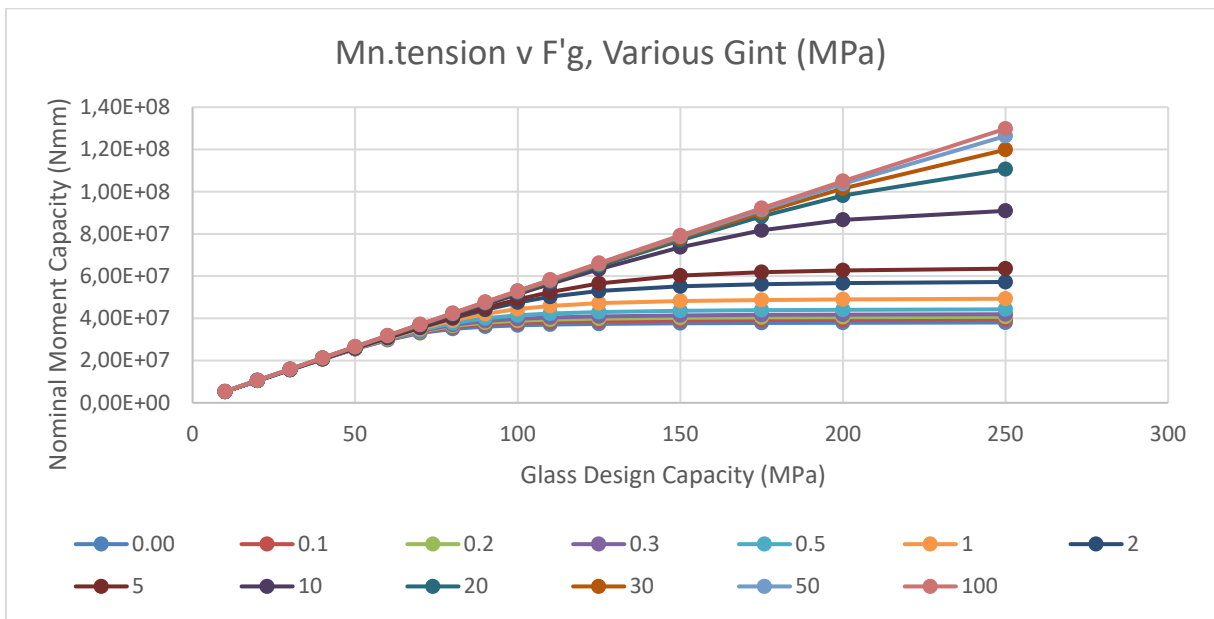


Fig. 10f: Nominal Moment Capacity (Nmm) with tension edge restrained vs Glass Design Capacity ( $F'g$ ) (MPa), for different shear moduli of the interlayer (MPa).

From Figures 10a and 10b, it can be observed that imperfections can significantly increase the stress for a given moment capacity approaching the buckling load, a phenomenon not captured in the AS1288 method.

From Figures 10c and 10d it can be observed that the introduction of any silicone bite has a significant effect and then added stiffness a lessor effect.

From Figures 10e and 10f, it can be observed that the shear stiffness of the interlayer has a significant impact on the moment capacity of the beam.

It should be noted that in Kala's derivation (Kala, 2013), initially both the lateral imperfection and the torsional imperfection are defined separately. In the final version of the formula, the torsional imperfection is assumed to be a function of the lateral imperfection. In benchmarking, the approximation works well for imperfections that resemble the primary buckling mode, including the number of wavelengths where appropriate, but can be somewhat conservative or non-conservative for other imperfections. To compensate, it is suggested to use a reduced  $M_{cr}$  to account for potential variations in the actual imperfection shape. A 15% reduction is proposed and has been found to be adequate for a limited number of checks for imperfections of practical magnitude but has not been tested exhaustively. Below, in figures 11b, 11c and 11d are examples of the comparison of the analytic method proposed here with finite element using layered brick models of the laminated glass fin, prepared using Strand7/Strauss7.

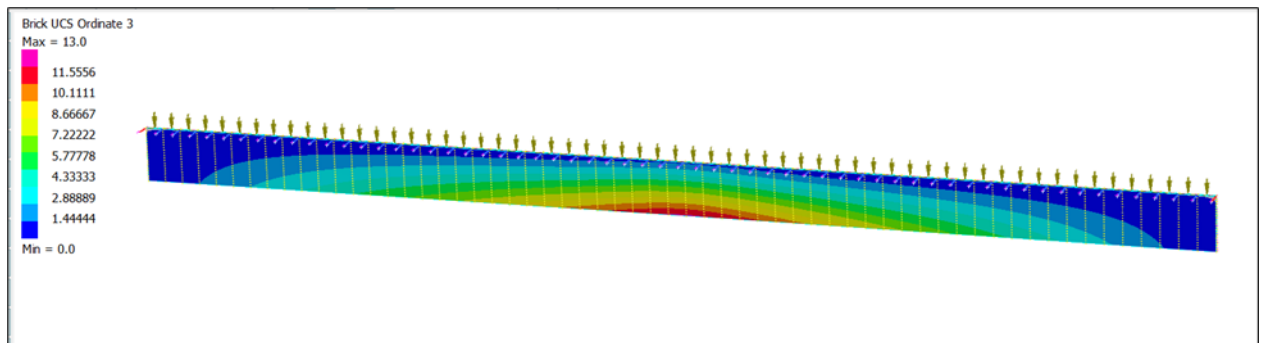


Fig. 11a: The seed imperfection was the primary buckling mode of the unbraced beam under negative load scaled to 12mm for all cases.

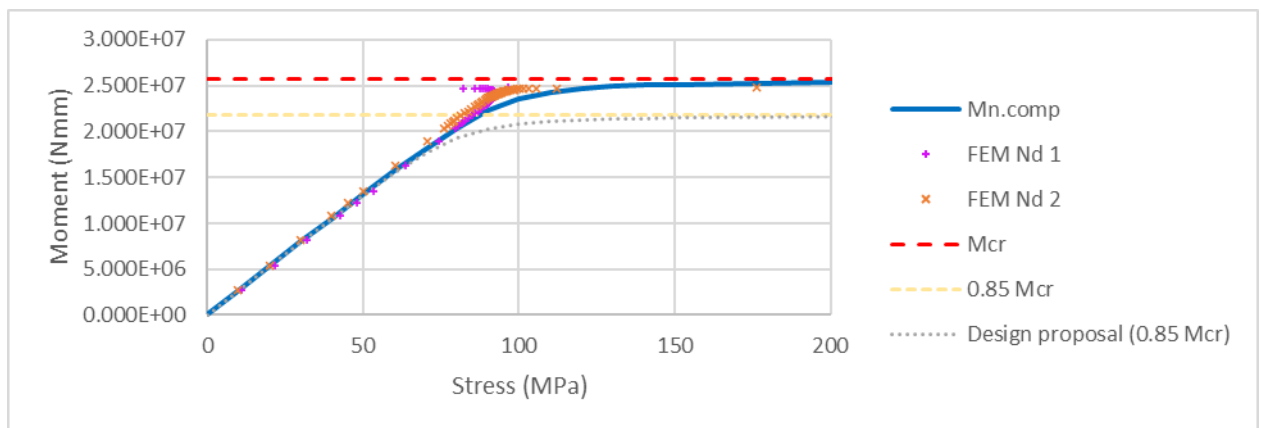


Fig. 11b: Comparison of finite element methods (FEM) and proposed methods for Nominal Moment Capacity vs Glass Design Capacity ( $F'g$ ), for elastic restraint to compression edge,  $G_{int} = 0.97$  MPa;  $k_x = 0.45$  N/mm/mm.

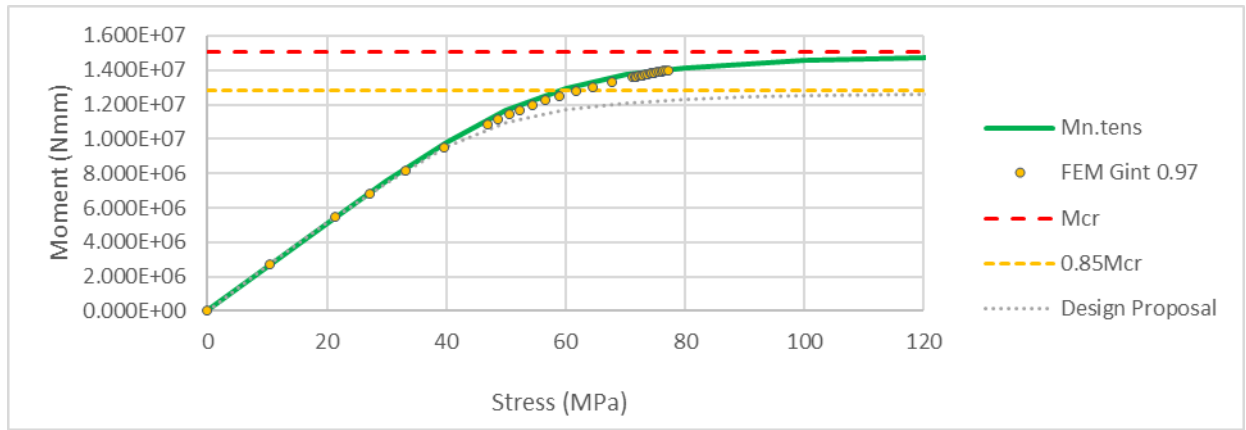


Fig. 11c: Comparison of finite element methods (FEM) and proposed methods for Nominal Moment Capacity vs Glass Design Capacity ( $F'g$ ), for elastic restraint to tension edge,  $G_{int} = 0.97$  MPa;  $k_x = 0.45$  N/mm/mm.

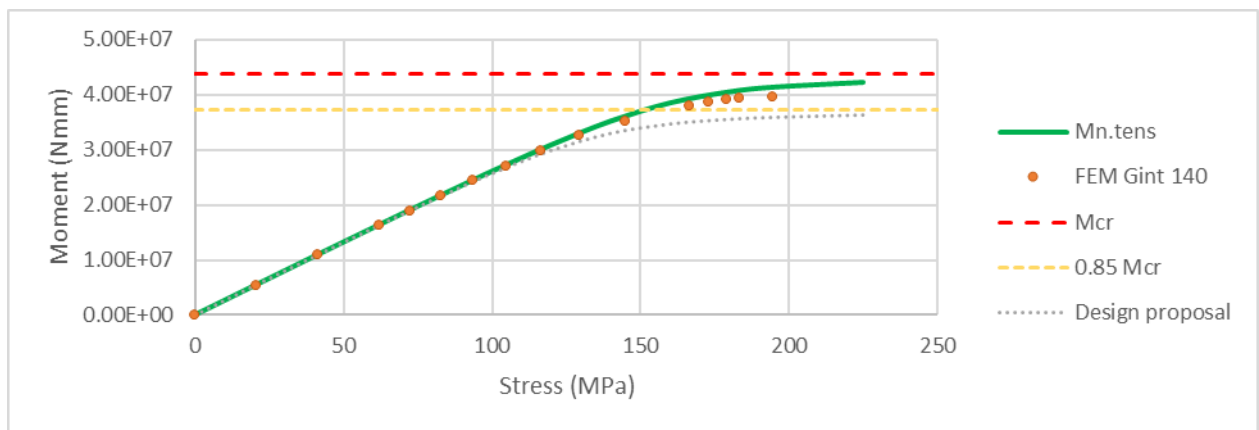


Fig. 11d: Comparison of finite element methods (FEM) and proposed methods for Nominal Moment Capacity vs Glass Design Capacity ( $F'g$ ), for elastic restraint to compression edge,  $G_{int} = 140$  MPa;  $k_x = 0.45$  N/mm/mm.

In figure 6b we see that because the seed imperfection poor, with widest imperfection at the tension edge and has a single half wave ( $n_R = 1$ ) whereas the critical elastic restrained mode has five half waves ( $n_R = 5$ ), there is a 'snap' from amplification of the initial imperfection to critical mode. Discrepancies between the theory and modelling in figures 6c and 6d also reflect the limitations of simple seed imperfections with lack of agreement to the critical case. See also section 6.

It is suggested for design to use a reduced elastic critical buckling moment in the Kala equation,  $M_{cr}^*$ , where  $M_{cr}^* = 0.85 M_{cr}$ .

Using  $M_{cr}^*$  with a 15% reduction also means that the Kala equation asymptotes to a capacity 15% below the elastic critical moment, hence no further reduction is required when design is performed to an LRFD (Load and Resistance Factor Design, i.e. limit state) level of load and stress capacity.

For LRFD strength capacity consider referencing EN 16612 or CEN/TS-19100. Note that the stress values in the appendix of ASTM E1300 are for statistically acceptable use in windows with limited consequence in the event of failure and are not indexed to an appropriate level of reliability for structural applications. Design to ASD (Allowable Stress Design) would require additional checks for buckling limits and design factor relative to wind load variation; alternatively the formula above can be used with  $M_{allow,ASD} = M_n / 1.6$ . (or appropriate weighted load factor).

## 7. Numerical Validation

In the comparisons below, it can be seen that the Kala equation (46) follows benchmark finite element models well for practical ranges of imperfections and moments less than  $0.85 M_{cr}$ . Above  $0.85 M_{cr}$  the finite element models will capture post-buckling behavior, whereas the Kala equation will asymptote to  $M_{cr}$ . Thus, the Kala equation has good accuracy at typical design levels of moment and is typically conservative where it deviates from actual.

To verify the accuracy of the analytical approach, a set of numerical simulations was carried out in ABAQUS software, by taking into account various geometrical and mechanical configurations of technical interest. The reference finite element (FE) model was described in ABAQUS according to Bedon et al. (2015) that is in the form of multilayer composite shell elements for the laminated glass section, with a set of springs to reproduce the adhesive joint. For the purpose of present comparison, both glass and interlayer materials were mechanically modelled as linear elastic. For a given geometrical and mechanical configuration, the typical analysis consisted in a nonlinear simulation with imposed initial imperfection and monotonically increasing bending moment for each beam. To account for the initial imperfection, the corresponding shape was Imported from a preliminary buckling analysis (Bedon et al., 2015). The subsequent nonlinear incremental analysis was thus carried out by monitoring the evolution of tensile stress peaks in glass, in order to capture the expected failure bending moment. Note that the initial imperfection shape was selected based on the critical buckling moment and on the corresponding number of half sine waves for each examined configuration.

Typical comparisons were carried out by monitoring the load-stress trend for selected configurations, as well as the failure bending moment for a given tensile strength. An example can be seen in Figure 7, where failure bending moments are compared for a multitude of input configurations in terms of analytical of FE numerical estimates for the selected laminated glass section (with 8 mm the thickness of three glass layers, 1.52 mm the thickness of interposed bonding films, with 0.3 m the height and 1/300 the initial imperfection). Different colors denote a variation in the stiffness of interlayers ( $G_{int}=3$  MPa or 7 MPa respectively).

In general, as in Figure 7, the percentage scatter of analytical and numerical predictions was measured in an average of less than 5%, and up to 8-9% for some cases. The comparative analysis showed that the softer is the interlayer and the higher is the calculated percentage scatter. In any case, the accuracy and robustness of the proposed analytical approach was emphasized by the measured limited scatter.

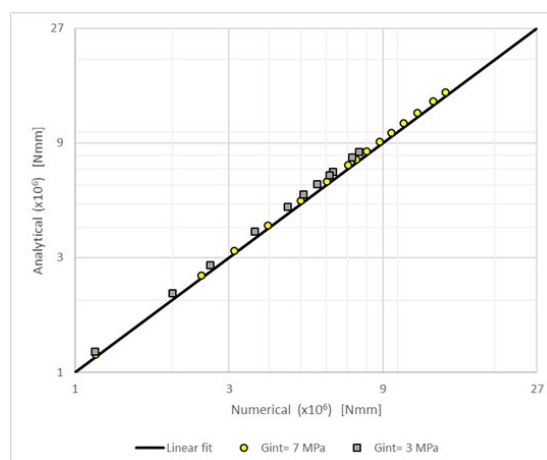


Fig. 12: Comparison of analytical and numerical failure bending moments for a selection of geometrical and mechanical configurations. In evidence, the effect of interlayer stiffness (with 1/300 the amplitude of initial imperfection).

The effect of initial imperfection, as previously discussed, has a critical role in load-bearing performance and bending capacity assessment. In this regard, Figure 8 shows that the selected numerical configurations – when affected by critical imperfection shape with a variable initial amplitude – are generally in good agreement with the corresponding analytical estimates. Especially for small initial imperfections (e.g., less than 1/300), the comparative results in Figure 8 have an associated scatter of less than 1%.

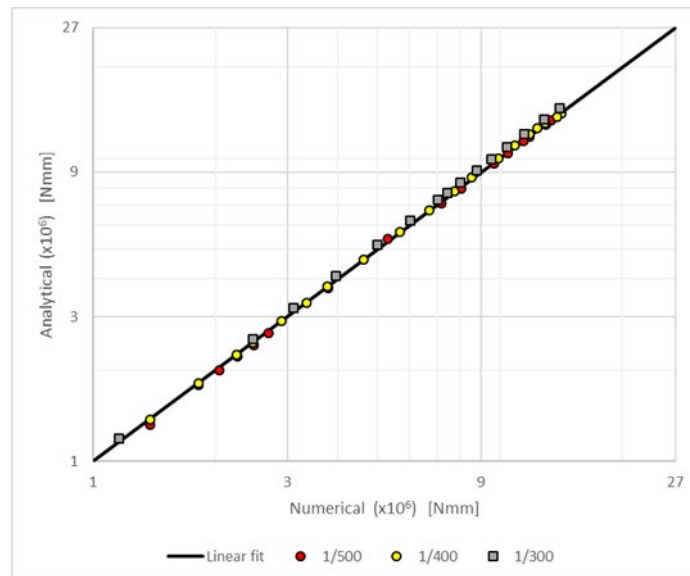


Fig. 13: Comparison of analytical and numerical failure bending moments for a selection of geometrical and mechanical configurations. In evidence, the effect of maximum amplitude for the initial imperfection (with  $G = 7$  MPa for the interlayer).

Finally, in accordance with Bedon et al., 2015, the shape of initial imperfection should be always associated to the critical number of sine waves to calculate conservatively the bending capacity of a given laminated glass beam. The use of first deformed shape ( $n_R=1$ ) for all configurations, would result in minimum 10% of overestimation of bending capacity relative to a matching seed imperfection or analytical approach (see for example Figures 6b, 6c, 6d and 9).

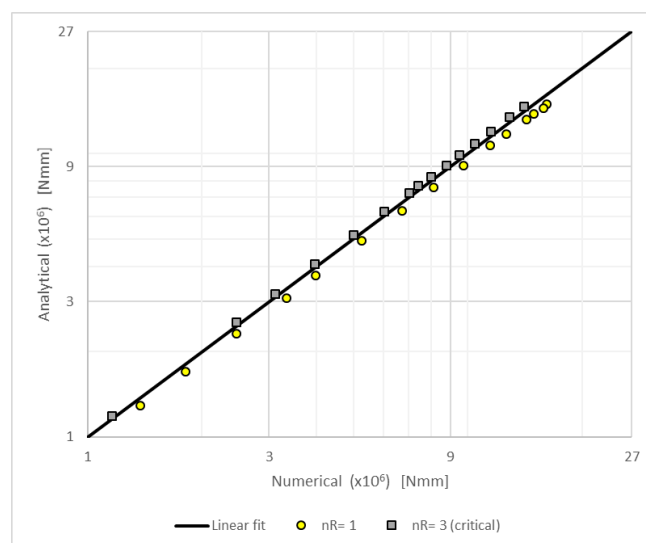


Fig. 14: Comparison of analytical and numerical failure bending moments for a selection of geometrical and mechanical configurations. In evidence, the effect of initial imperfection shape and sine waves  $n_R$  (with  $G = 7$  MPa for the interlayer and 1/300 the amplitude of initial imperfection).

## 8. Summary

The stability equations in AS1288 for continuous restraint have been found to be non-conservative for some circumstances such as continuous elastic restraint by structural silicone. Glass is brittle and laminated glass is a popular method to add robustness and control the behaviour of glass beams if they are damaged by non-design loads. The Wolfel-Bennison effective thickness model in ASTM E-1300 is non-conservative for torsional stiffness (if the beam length is used for 'a') and hence is non-conservative for stability calculations of laminated glass fins. As imperfect beams approach the critical elastic buckling moment, secondary stresses may develop that are significant relative to the tensile capacity assumed for the glass. AS1288 has been used successfully for monolithic fins because the strength model for structural fins in that standard is more conservative than others; the conservative strength model makes allowances for the other inaccuracies.

The method presented includes treatment of glass fins that are monolithic or laminated, unrestrained or with continuous elastic lateral restraint, taking into account the effect of imperfections in a system and the increase in stress they cause as loads approach the elastic critical buckling moment.

The Enhanced Effective Thickness method by Galuppi et al. has been presented with an alternate formulation that unifies the form of the equation for each of the target stiffnesses being considered, introducing a new term, and allowing the rest of the equation to be standardized. This also allows unification of the 2-ply, 3-ply and N-ply formulations previously presented by Galuppi into a single equation.

The formulas for elastic critical buckling moment for beams with continuous elastic restraint on the compression and tension flange by Bedon et al. have been unified into a single equation. The critical load profile for beams with non-uniform moment has been identified as the moment on the half wavelength rather than the overall beam.

When calculating the effective section stiffnesses for laminated beams, the characteristic length parameter for buckling is the distance between the points of contra-flexure, i.e. the half-wavelength, not the overall beam dimensions.

The Kala formula for imperfect beams has been introduced as a tool for calculating the moment capacity of glass beams given a target stress, critical elastic buckling moment, and initial imperfection.

The method of analysis has been found to be favourably accurate for the practical design ranges of moment, less than  $0.85 M_{cr}$ . Above this moment the comparison with finite element analysis is highly subject to the shape of the initial imperfection modelled, which in reality will also be unknown; thus, a reduction factor on  $M_{cr}$  is proposed to allow for practical design.

The method increases the accuracy of fin and beam moment capacity, taking into account lamination, continuous elastic lateral restraints, stress capacity, and initial imperfections.

## Declaration

On behalf of all authors, the corresponding author states that there is no conflict of interest. No funding was received to assist with the preparation of this manuscript.



## References

- ANSI/AISC 360 Specification for Structural Steel Buildings. American Institute of Steel Construction
- ASTM E1300 (2016)- Standard Practice for Determining Load Resistance of Glass in Buildings, ASTM International, West Conshohocken, PA, USA
- Australian Standard AS1288 (2021) Glass in Buildings – Selection and Installation, Standards Australia, GPO Box 476 Sydney, NSW 2001, Australia
- Australian Standard AS4100 *Steel Structures*, Standards Australia, GPO Box 476 Sydney, NSW 2001, Australia
- Bedon, Chiara, Belis, Jan, and Amadio, Claudio (2015). Structural assessment and lateral-torsional buckling design of glass beams restrained by continuous sealant joints. *Engineering Structures*, 102 (11): 214-229.
- Bedon, Chiara (2021). Lateral-torsional buckling (LTB) method for the design of glass fins with continuous lateral restraints at the tensioned edge. *Composite Structures*, 266: 113790.
- CEN/TS 19100-1 Design of glass structures— Part 1: Basis of design and materials
- D’Ambrosio, Gianmaria, and Galuppi, Laura (2020). Enhanced effective thickness model for buckling of LG beams with different boundary conditions. *Glass Structures & Engineering*, 5(2): 205-210
- Dumont C. (1937) NASA N.A.C.A. Technical Note No 601 *The Lateral Instability of Deep Rectangular Beams* <https://ntrs.nasa.gov/citations/19930081361>
- EN 16612: Glass in building. Determination of the lateral load resistance of glass panes by calculation
- EN 1993-1-1: Eurocode 3: Design of steel structures— Part 1-1: General rules and rules for buildings
- Galuppi, Laura, Manara, Giampiero, and Royer-Carfagni, Gianni (2013). Practical expressions for the design of laminated glass. *Composites: Part B*, 45: 1677–1688
- Galuppi, Laura, and Royer-Carfagni, Gianni (2014). Enhanced Effective Thickness of multi-layered laminated glass, *Composites: Part B*, 64: 202–213
- Galuppi, Laura, and Royer-Carfagni, Gianni (2020). Enhanced Effective Thickness for laminated glass beams and plates under torsion. *Engineering Structures*, 206: 110077.
- Green, R., Bedon, C., Galuppi, L., (2023) Design and stability of laminated glass fins with continuous lateral silicone restraint 2023 *Glass Structures and Engineering* 8(3):1-20 DOI: <http://dx.doi.org/10.1007/s40940-023-00224-1>
- Kala, Zdeněk (2013). Elastic Lateral-Torsional Buckling of Simply Supported Hot-Rolled Steel I-Beams with Random Imperfections. *Procedia Engineering* 57: 504-514.
- Kraus, Crisan and Wittor (2021) *Stability Study of Cantilever-Beams – Numerical Analysis and Analytical Calculation (LTB)*. CE/Papers <https://d-nb.info/125069664X/34>
- NCCI SN-003-EN-EUNCCI: Elastic critical moment for lateral torsional buckling, by Access Steel. <https://eurocodes.jrc.ec.europa.eu/doc/WS2008/SN003a-EN-EU.pdf>
- Nethercott D.A., Rockey K.C. (1971), "A unified approach to the elastic lateral buckling of beams", *The Structural Engineer*, 49:321–30
- Nethercott, D.A., and Trahair, N.S. (1976). "Inelastic lateral buckling of determinate beams", *Journal of the Structural Division*, ASCE, 102 (ST4)
- Nizich, Adam J, La Greca, Andrea M and Galuppi, Laura. Advances in Effective Thickness For Laminated Glass Structural Design, Facade Tectonics Institute's biennial World Congress, 2022
- Simulia (2022), ABAQUS computer software, v.6.14, Providence, RI, USA
- SN006a-EN-EU NCCI: Elastic critical moment of cantilevers. Access Steel
- Strand7 finite element software, R3.1.1, Sydney, NSW, Australia. <https://www.strand7.com/>
- Timoshenko and Gere *Theory of Elastic Stability* (1956)

## Platinum Sponsor

---



## Gold Sponsors

---



## Silver Sponsors

---



## Organising Partners

---

